Chem Soc Rev

REVIEW ARTICLE

View Article Online
View Journal | View Issue



Cite this: *Chem. Soc. Rev.*, 2024, **53**, 3065

# Water structures on acidic zeolites and their roles in catalysis

Qiang Liu [a] and Jeroen A. van Bokhoven *[ab]

The local reaction environment of catalytic active sites can be manipulated to modify the kinetics and thermodynamic properties of heterogeneous catalysis. Because of the unique physical–chemical nature of water, heterogeneously catalyzed reactions involving specific interactions between water molecules and active sites on catalysts exhibit distinct outcomes that are different from those performed in the absence of water. Zeolitic materials are being applied with the presence of water for heterogeneous catalytic reactions in the chemical industry and our transition to sustainable energy. Mechanistic investigation and in-depth understanding about the behaviors and the roles of water are essentially required for zeolite chemistry and catalysis. In this review, we focus on the discussions of the nature and structures of water adsorbed/stabilized on Brønsted and Lewis acidic zeolites based on experimental observations as well as theoretical calculation results. The unveiled functions of water structures in determining the catalytic efficacy of zeolite-catalyzed reactions have been overviewed and the strategies frequently developed for enhancing the stabilization of zeolite catalysts are highlighted. Recent advancement will contribute to the development of innovative catalytic reactions and the rationalization of catalytic performances in terms of activity, selectivity and stability with the presence of water vapor or in condensed aqueous phase.

Received 16th October 2023

DOI: 10.1039/d3cs00404j

rsc.li/chem-soc-rev

[a] *Institute for Chemical and Bioengineering, ETH Zurich, Vladimir Prelog Weg 1, 8093 Zurich, Switzerland. E-mail: jeroen.vanbokhoven@chem.ethz.ch*
[b] *Laboratory for Catalysis and Sustainable Chemistry, Paul Scherrer Institut, 5232 Villigen PSI, Switzerland*

## 1. Introduction

The variations of the local environment near heterogeneous catalyst surface make it possible to manipulate catalytic

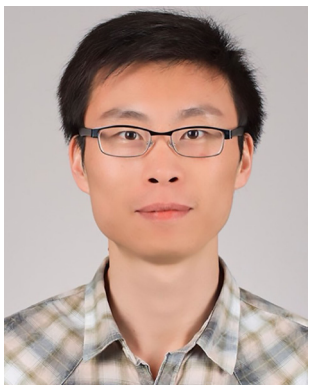

**Qiang Liu**

*Qiang Liu received his PhD degree of Chemical Engineering from Qingdao Institute of Bioenergy and Bioprocess Technology, Chinese Academy of Sciences in 2018. He worked as a postdoc student in the research group of Prof. Johannes A. Lercher at Technical University of Munich (TUM) from 2018 to 2020. Then, he came to work with Prof. Jeroen A. van Bokhoven at ETH Zurich and Paul Scherrer Institute as a postdoctoral fellow. His current research interest focuses on the design of advanced nanocatalysts and their related applications in heterogeneous catalysis.*

**Jeroen A. van Bokhoven**

*Jeroen A. van Bokhoven completed a degree in chemistry at Utrecht University (Netherlands) in 1995 and went on to obtain a PhD in inorganic chemistry and catalysis from the same university in 2000 (with honours). From 1999 until 2002, he was head of the XAS (X-ray absorption spectroscopy) users-support group at Utrecht University. In 2002, he moved to the ETH Zurich, where he worked as a postdoctoral researcher in the group of Professor Prins. In 2006 he obtained an SNF assistant professorship in the Department of Chemistry and Applied Biology. He was the 2008 recipient of the Swiss Chemical Society Werner Prize. Since 2010, Jeroen A. van Bokhoven has a Chair in Heterogeneous Catalysis at the Institute for Chemical and Bioengineering at ETH Zurich and is Head of Laboratory for Catalysis and Sustainable Chemistry at Paul Scherrer Institute.*

chemistry.[1–3] A catalytic reaction usually involves active sites, reactants, reactive intermediates, products and solvent (if involved). Water acts as either a co-feed reactant, or a co-product of the reaction or the solvent from condensed aqueous phase for a number of surface-catalyzed chemical transformations. The critical role of water in heterogeneous catalytic reactions at the solid–gas and solid–liquid interfaces has recently become an important topic in catalysis research.[4–6] Water molecules adsorbed/existed within the microenvironment of active sites can mediate the sorption behavior of reactants and surface intermediates on the surface of heterogeneous catalysts, leading to tailored reaction pathways and distinct catalytic performances.[7–10] The nature as well as the structure of active sites on solid catalysts can be altered by the presence of water molecules, thus making differences in the activation energy barrier of the elementary steps for a catalytic reaction.[11] On the other hand, the promotional effects of water in terms of the solvation of reaction partners, the influences on the surface chemistry of active sites and the stabilizations of surface intermediates and activated complexes, have been identified as well.[12,13] Performing heterogeneous catalytic reactions in aqueous phase appears to be profitable for reducing energy input (low reaction temperature), and achieving high catalytic reaction rate and product selectivity, which are different from those of gas-phase reactions.[14,15] It is noteworthy that an aqueous phase environment usually complicates the understanding of the specific interactions of solvent molecules with reactants and active sites, thus bringing challenges to the insights of reaction mechanisms and structure–performance relations.[3,16] Apart from these above, the influence of water on the structural and chemical stability of solid catalysts, *e.g.*, crystalline microporous zeolites should be additionally considered for their efficient applications in heterogeneous catalysis.[17,18]

Zeolitic materials, Brønsted- and Lewis-acidic tectosilicates, are built up from $SiO_4$ tetrahedra to feature an ordered distribution of micropores with the molecular dimensions.[19,20] Since the report of one of the first synthetic zeolites, aluminosilicate mordenite (MOR),[21] a great number of zeolites have been developed and deployed in petrochemical industry, mostly for catalysis, separation and sorption.[22–24] The confinement in the zeolite pores is vital to affect the sorption energetics of reacting molecules, facilitate the dispersive interactions of reactive intermediates and transition states within zeolite channel structure.[25–27] Besides, the nanoscopic environments in zeolite structures vary with the confined species and the hydrophilic/hydrophobic nature of the micropores, which eventually determine the reaction pathways and thus the reaction rates and catalytic efficiencies.[28,29] Zeolites are effective heterogeneous catalysts for catalyzing a wide variety of chemical reactions, particularly performed in the presence of water. Water molecules can be initially stabilized on Brønsted acid sites, framework heteroatom metal sites and structural defects, followed with the formation of hydrated hydronium ion clusters and extended hydrogen-bonded water networks, which differ substantially from the bulk water. Intraporous water structures occluded in the zeolite pores could make distinct differences for heterogeneous catalysis. Understanding about the formation of water structures in zeolite pores and the corresponding functions in catalytic reactions are desirable to gain the fundamental bases for enhancing catalytic reaction rates and efficiencies at the solid–gas and solid–liquid interfaces. Brønsted and Lewis acidic zeolites will be the focus of this Review, given their wide applications in the development of renewable catalytic processes for transportation fuels and valuable chemicals. The roles of water in metal-containing zeolites-catalyzed reactions (*e.g.*, methane oxidation to methanol,[30–32] selective catalytic reduction of nitrogen oxides (SCR-$NO_x$),[33,34] Wacker oxidation of ethylene,[35,36] high-temperature alkane conversion and biomass valorization[37]) and water effects in the dynamic evolution of metal sites confined in zeolite structures are beyond the scope of the present Review. Detailed progress on the latter respect can be found from a recently published Review paper by Hu *et al.*[38]

Recently, the research group of Resasco provided comprehensive reviews of water-mediated heterogeneous catalysis[4] and the interactions of water with zeolites.[39] Stanciakova *et al.* reviewed the water-active site interactions in zeolites based mostly on the viewpoint of molecular modeling approaches.[18] In addition, Lin *et al.* briefly summarized the positive effects brought with water molecules on traditional heterogeneous catalytic reactions, such as aqueous-phase reforming, aqueous-phase methane activation and aqueous-phase Fischer–Tropsch synthesis catalyzed by noble metal or transition metal nanoparticle-based materials.[5] Nonetheless, it should be pointed out that advances in the nature and structures of microscale intrazeolite water on the surface of both Brønsted and Lewis acidic zeolites, and the consequent various functions of water structures in zeolite catalysis have not been well summarized in previous works. In the present Review, we first showcase the adsorption behaviors of water from the gas and aqueous phase, and the resulted structural properties of water confined in zeolitic materials. After that, we stress the critical roles of water in impacting the heterogeneously zeolite-catalyzed reactions in terms of the chemical thermodynamics, catalytic reactivity and catalytic/structural stability. Considering that the stability of zeolite materials with the presence of water is of great importance, the potential strategies developed to contribute to zeolite stabilization are also described. Advancements in the research outlined above could distinguish this work from the previous reviews and enlarge the research progress of understanding water-active site interactions on a variety of acidic zeolites. Finally, future research perspectives associated with zeolite catalysis involving the specific interactions between zeolite framework and water structures are highlighted.

## 2. Water structures on acidic zeolite materials

### 2.1. Brønsted acidic zeolites

For aluminosilicate zeolites, substituting tetrahedrally coordinated $Si^{4+}$ with typically $Al^{3+}$ heteroatom results in the

 

formation of Brønsted acid site (BAS), that is, a hydroxyl group is bridged an aluminum and silicon atom in case of protons as charge balancing cation (Si(OH)Al).[40] Aluminosilicate zeolites are the most relevant active materials for catalyzing the reactions including hydrocarbon conversions, such as cracking[24,40,41] and isomerization,[40] and alkylation,[11] alcohol dehydration,[42,43] ketonization,[44,45] and esterification reactions.[46] Silicoaluminophosphate (SAPO) molecular sieves such as SAPO-34 is another class of microporous crystalline material, which are widely applied in the methanol-to-olefins (MTO) conversion.[22,47,48] The Brønsted acid sites in SAPO molecular sieves are generated by the incorporation of Si into $AlPO_4$ structures with the presence of charge compensation cations, *i.e.*, protons. Zeolite Si(OH)Al groups usually manifest strongly covalent character in the absence of adsorbates in the pores. With the presence of adsorbates inside of zeolite structures, the polarity of OH bond increases due to the acid–base interactions through hydrogen bonding (H-bonding).[49] The protonation of substrate molecules of different base strength by the BAS on the surface or pore of zeolites often constitutes as the initial step for solid acid-catalyzed reactions. Water ($H_2O$), as a good proton acceptor, is employed in general to get insights into the fundamental aspects in terms of the nature of zeolite acidity and the protonation ability of the BAS of zeolite.[50–53] Intensive research works have pointed to study the interactions of water molecules with the BAS on Brønsted acidic zeolites in the past decades. The adsorption behavior of water molecules and the structural configuration of water clusters on zeolitic Brønsted acid sites will be briefly summarized.

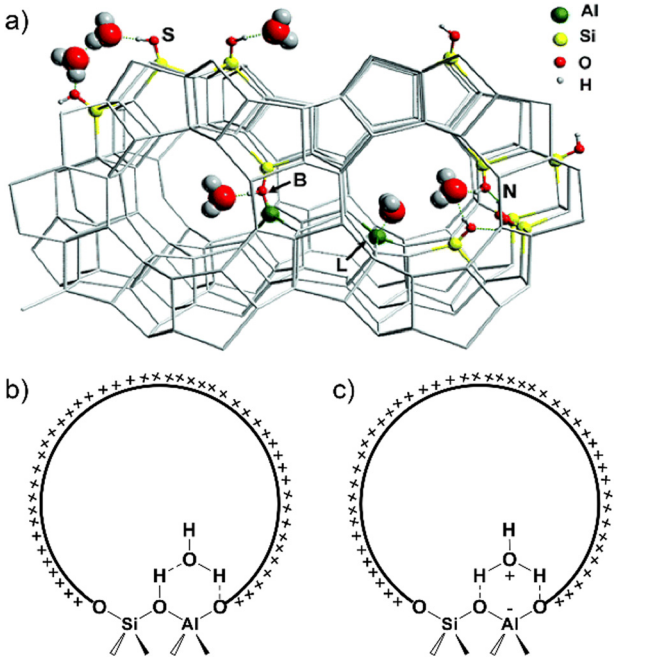


Fig. 1 (a) Possible interactions between water molecule and (acidic) sites in H-MFI zeolite cavities. B: Brønsted acid site, L: Lewis acid site, N: silanol nests, S: external surface Si–OH groups. Reproduced with permission from ref. 54. Copyright 2006, American Chemical Society. Structural model of water adsorption in H-form zeolite pore: (b) hydrogen-bonded model; (c) protonated model. Dashed lines represent the formation of hydrogen bonds between water species and zeolite framework.

**2.1.1. Monomeric and dimeric water-proton complexes formed on Brønsted acidic zeolite.** The BAS, Lewis acid site (*i.e.*, Al(III)) and Si–OH species including silanol nests at the internal surface and isolated silanols at the external surface are among the coordination sites for water adsorption (Fig. 1a).[54] The coordination of water molecules with the BAS through forming strong H-bonding are dominant on the surface of Brønsted acidic zeolites.[50] Fourier-transform infrared spectroscopy (FT-IR) and magic-angle spinning (MAS) nuclear magnetic resonance (NMR) experimental technologies along with theoretical calculations have been conducted with the purpose of investigating the interactions between water molecules and Brønsted acidic zeolites.[55,56] In an earlier work by analyzing the time-resolved FT-IR, Jentys *et al.* suggested that absorbate molecules (*e.g.*, water) could initially form 1 : 1 complexes (one water molecule per BAS) on the acidic site of H-ZSM-5 zeolite (ZSM-5: Zeolite Socony Mobil-5).[57] It resulted in the disappearance of the bond of bridging hydroxyl at 3609 $cm^{-1}$, followed by formation of bonds at ~2900 $cm^{-1}$ (A band) and ~2400 $cm^{-1}$ (B band) due to the H-bonding of BAS with the water molecule.[58,59] For a long time, the structure of single water adsorption on Brønsted acidic zeolites has been debated. Adsorption of a single water molecule on the BAS site of zeolite could create a structure that features a hydrogen-bonded model (Fig. 1b),[60,61] a protonated model (Fig. 1c)[62] or the hydrogen-bonded model co-existed with the protonated one.[51,63,64] FT-IR on $H_2{}^{18}O$ adsorption on H-ZSM-5 has provided spectroscopic evidence for the generation of hydrogen-bonded neutral adduct in the process of the adsorption of the single water molecule.[65] Car–Parrinello molecular dynamics demonstrate that the water molecule forms a strong H-bond with the OH group of the BAS and a weak H-bond with a second neighboring oxygen atom in the framework of zeolite chabazite (CHA, H-SSZ-13).[66] The hydrogen-bonded water-proton complex has been identified as the favorable model by far for the special interaction of a single water with the BAS on Brønsted acidic zeolites.[66–68] Upon interacting with a single water, the proton from the BAS cannot be sufficiently stabilized; instead, the adsorbed water molecule is hydrogen-bonded to the Si(OH)Al site as a neutral complex without the proton transference from zeolite framework in the pores.[68,69]

Increasing the dose of water on Brønsted acidic zeolites could convert the monomeric water complex to dimeric species. The dimeric water was predominately assigned to be stable $H_5O_2^+$ species (that is the typical "Zundel" cation) by the aid of FT-IR spectra[58,70,71] and temperature-programmed desorption analysis.[72] Comparatively, NMR and molecular dynamics studies have suggested that the proton involved in the dimeric water structures can be transferred from the framework Si(OH)Al group to the sorbed water molecules,[73,74] because water dimer has a higher value of proton affinity (806 kJ $mol^{-1}$) than the water monomer (694 kJ $mol^{-1}$).[63] Water dimer, as the most stable equilibrium structure based on the PBE (Perdew, Burke and Ernzerhof) function, is able to deprotonate the

bridging hydroxyl on the zeolite such as H-SSZ-13.[66] The as-formed $H_5O_2^+$ species comprising a hydronium ion core ($H_3O^+$) and the second hydrogen-bonded water are ion-paired with the framework aluminum sites on H-ZSM-5 zeolite.[68] Notably, these $H_5O_2^+$ species show quite low stability according to the observations from density functional theory (DFT) optimization, where the protons undergo dynamic rearrangement between the BAS and $H_5O_2^+$ in the zeolite pores. In addition to proton affinity, the loading of water and temperature are the critical aspects that determine the degree of the protonation of water structures by the zeolitic BAS.[53,63,75] It has been known that water adsorption uptakes in zeolite pores are proportional to the content of framework aluminum atoms in H-form zeolitic materials.[54,76–78] Ion-paired hydronium ions with higher protonation degree and larger cluster size can be created upon the stepwise adsorption of three or more water molecules on the framework aluminum sites of Brønsted acidic zeolite (*vide infra*). Meanwhile, the H-bonding interactions between water clusters and zeolite framework and those within water clusters tend to decrease with increasing temperature, as indicated by the study using reactive force field (ReaxFF) method.[75] Moreover, zeolite topology often affects the formation and stabilization of protonated water adducts in the zeolite pore networks; protonated water clusters with more than two water molecules are susceptible to be stabilized in small-pore zeolites.[49,66,67,79] Brønsted acidic zeolites with unique water structures adsorbed on their frameworks most probably exhibit differently affected catalytic performance, which will be discussed in section 3 dedicated to catalytic roles of water–zeolite interactions.

**2.1.2. Hydrated hydronium ion clusters confined in Brønsted acidic zeolite.** An increased hydration degree of Brønsted acidic zeolite gives rise to the formation of hydronium ion species ($H^+(H_2O)_n$), in particular, in hydrophilic micropores.[71,80–82] *Ab initio* dynamics simulations (AIMD) at different level of theory (*e.g.*, generalized gradient approximation (GGA),[73,83] Perdew–Burke–Ernzerhofer (PBE) functional[66,84]) revealed that large-sized water clusters, *e.g.*, water trimers possess a high electron density and thus the proton affinity high enough to become protonated in the pores of zeolite such as H-SAPO-34 (silicoaluminophosphate of CHA),[73,83] H-SSZ-13[66] and H-MFI.[84] In the work of Hack *et al.*,[85] it was suggested that water trimer is the smallest cluster and a triply coordinated water molecule is the important structural motif to stabilize proton in zeolite pores. The acidic protons in water clusters usually have a high probability of moving away from the framework aluminum sites[75,82] or even entering into the water-filled pores[86] and the protonated water clusters can serve as the catalytically active species in different zeolites.[87] Similar to water dimer, the protonated water clusters comprising of high water loadings (*e.g.*, 8 : 1 and 10 : 1 ratios of water to aluminum) are not stable and the acidic protons could move back to zeolite framework at elevated temperature.[75] A recent study by Wang *et al.* provided experimental evidence for the nature and stability of hydronium ions formed in the hydrated H-ZSM-5 zeolite channels.[88] The generation of a hydronium ion when more than two water molecules interact with the BAS in zeolite is unambiguously indicated by the 9-ppm signal in $^1$H NMR spectra (Fig. 2a). In the $^1$H-$^{29}$Si cross polarization NMR spectra collected with increasing water loading on the surface of acidic zeolite, the mobility of the protonated water cluster starts to be promoted, even with the presence of two water molecules on BAS site. Molecularly-confined water clusters tend to have high proton affinities and facilitate the delocalization of the protons of hydroxyl groups (Si(OH)Al) from the zeolite framework in the form of $H^+(H_2O)_n$.[88] The authors also used periodic DFT-based AIMD at the GGA level of theory to calculate the probability of distance between the oxygen atoms and the center of mass (COM) for the system in H-ZSM-5 and another system of protonated eight water molecules in the gas phase. Calculation results suggested that the zeolite-confined water clusters are chemically different from those in case of gas phase without confinement; in particular, water clusters in the zeolite micropores are more compressed and feature with an enhanced proton mobility. Above established findings have been confirmed by inelastic neutron scattering as well as AIMD (at the GGA level) in the work of Jiménez-Ruiz *et al.*[69]

The composition of $H^+(H_2O)_n$ in zeolites can be measured from water vapor adsorption isotherms by the means of thermogravimetric analysis. Both the BAS and silanol groups (*i.e.*, the external silanol and internal defect sites) on zeolite surface serve as the stabilization sites for water molecules. In addition, the density of silanol groups usually relies on the synthetic parameters and the structural properties of resulting zeolitic materials. These thus lead to differences in the quantification of the number of adsorbed water per acid site on Brønsted acidic zeolites.[89,90] For example, Chen previously reported a stoichiometric ratio of four water molecules on each framework aluminum from the water adsorption isotherm at a relative pressure $P/P_0$ of 0.6.[91] Zechhina *et al.* obtained an averaged three-to-five interval of water molecules for the $H^+(H_2O)_n$, by normalizing the total number of water filled in zeolite pores to the number of BAS site.[49] Olson *et al.* identified the tetrahydrate of the proton, $H_9O_4^+$, as the stable water ionic complexes in H-ZSM-5 with the Si/Al ratios range from 37.5 to 4330.[77] A relatively high ratio of five water molecules per the site of framework aluminum on zeolite H-ZSM-5 was observed from the work of Sano *et al.*[92,93] Moreover, Chen *et al.* found that the size of water clusters formed around each acid site of H-MFI zeolite varied with the density of acid sites.[94] Zeolites with a Si/Al ratio of 140 typically showed an adsorption capacity of around eight water molecules per the acid site.

Very recently, Eckstein *et al.*[95] reported a composition of $7 \pm 1$ water/BAS by subtracting the amount of water adsorbed on the defect sites of H-ZSM-5 zeolite based on the data from Olson and Sano.[77,92,93] The authors also researched the gas-phase water adsorption on series of H-MFI zeolites by stepwise dosing water vapor until adsorption saturation (31.6 mbar) at 25 °C. Water adsorption uptake for the hydrophobic silicalite-1 was determined to be one water molecule per unit cell. The BAS on zeolite H-MFI eventually function as the selective adsorption

 

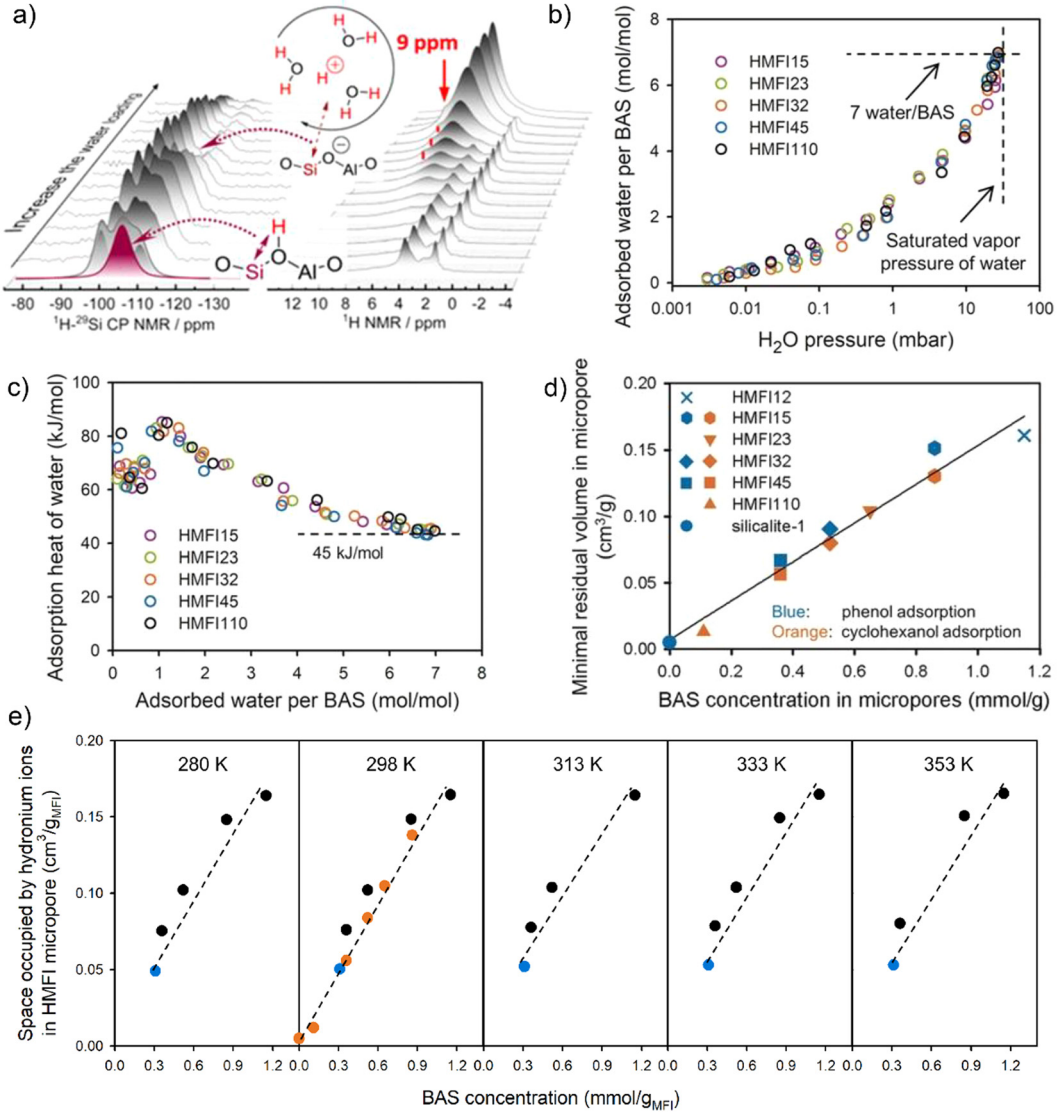


Fig. 2 (a) $^1$H and $^1$H-$^{29}$Si CP NMR spectra collected with increasing of water loading on H-MFI zeolite (Si/Al = 15 or 40). Reproduced with permission from ref. 88. Copyright 2019, American Chemical Society. (b) Gas-phase water adsorption isotherms on various H-MFI zeolites (Si/Al = 15, 23, 32, 45, 110) at 298 K, with the value of uptake normalized to the concentration of the BAS. (c) The adsorption heat of water as a function of the number of water per BAS. (d) The micropore space volume occupied by water in zeolite H-MFI at the saturated adsorption of cyclohexanol and phenol in the aqueous phase. Reproduced with permission from ref. 95. Copyright 2019, Wiley-VCH. (e) The space occupied by hydronium ions in zeolite H-MFI micropores as a function of BAS concentration at different temperatures. Reproduced with permission from ref. 99. Copyright 2021, AAAS.

sites for water molecules from the gas phase. An identical adsorption isotherm was obtained by normalizing the amount of adsorbed water to the concentration of the BAS site (Fig. 2b). Hydronium ion cluster comprising of one proton and seven water molecules can be generated at the stage of the saturation of water vapor. The adsorption heat for the first water on BAS is about 65 ± 5 kJ mol$^{-1}$ (Fig. 2c). With increasing the number of water adsorbed on the acidic sites, water adsorption heat firstly increases to 85 kJ mol$^{-1}$ and then presents a decreasing trend to 45 kJ mol$^{-1}$ which is consistent with the water condensation heat ($\Delta H$ = 43.5 kJ mol$^{-1}$) at 30 °C. In the work of Bates *et al.*,[96] the intracrystalline water structures on H-BEA zeolites with 0.11 to 2.0 proton per unit cell were studied by means of the gas-phase adsorption isotherms and *in situ* IR spectroscopy. At low water partial pressure ($P/P_0$ < 0.2), the generation of $(H_3O^+)(H_2O)_{6\pm1}$ clusters on the acidic sites of H-BEA was favored, whereas extended hydrogen-bonded networks started to be formed within the pores at $P/P_0$ > 0.2. In order to precisely quantify the structure of hydronium ions confined in the pores of H-BEA, Kim *et al.*[97] synthesized a wide range of H-BEA materials with varied BAS concentrations and minimized amount of defect sites. In this work, each hydronium ion is measured to be composed of 10 water molecules and one proton ($H^+(H_2O)_{10}$). This also contradicts with the result from DFT calculations on H-BEA previously performed by Mei *et al.*[80] Such discrepancy indicates that the composition of hydronium

ion clusters is likely dependent on the zeolite topologies. According to Kim *et al.*,[97] the larger size of hydronium ions in H-BEA than those in H-ZSM-5 resulted from the lower entropy loss in larger H-BEA pores.

The composition of water clusters in zeolite pores can also be measured by the saturated adsorption uptake of organic substrate, *e.g.*, cyclohexanol in aqueous phase.[95] Assuming the packing density of hydronium ion equals to that of free water, the volume of hydronium ions is the difference between micropore volume of zeolite and volumetric uptake of organic adsorbates. A linear correlation of the volume of hydronium ion with respect to the concentration of BAS on H-ZSM-5 zeolites was reported by Eckstein *et al.* (Fig. 2d).[95] The composition of hydronium ions confined within the H-ZSM-5 micropores is $H^+(H_2O)_{7\pm1}$, which is consistent with that measured from gas-phase water adsorption. As further indicated in the study of Grifoni *et al.*[98] by the means of *ab initio* metadynamics calculation at the PBE + DFT-D2 level (D2: Grimme's second-generation dispersion corrections), water clusters fabricated around the BAS of H-ZSM-5 bring out limited size because of the decreased stabilization by the inner energy of water molecules that are hydrogen-bonded in the hydrated hydronium ion clusters. By examining a selected group of zeolite frameworks (MFI, CHA, FAU, GIS), the authors demonstrated the minor role of zeolite confinement in determining the structural behavior of water clusters and the adsorbed water molecules are primarily surrounded the BAS without far away diffusion in the zeolite cavities.

Each hydronium ion cluster ($H^+(H_2O)_8$) has been determined to occupy a volume of (239 ± 15) Å$^3$ in the micropores of zeolite H-MFI with varied Si/Al ratios.[95] Based on the diameter of H-MFI zeolite cavities (5.6 × 5.4 Å in diameter for the 10-membered ring channels), a cylindric model was assumed for $H^+(H_2O)_8$ cluster with a radius of *ca.* 2.8 Å and a length value of about 10 Å. This implies that the hydrated hydronium ions are tightly confined in zeolite micropores. In addition, the hydronium ions confined inside of the H-MFI pores are stable with respect to their composition at the temperature between 280 and 353 K (Fig. 2e).[99] The formation of a stable $H^+(H_2O)_8$ water cluster has been confirmed by the calculated radial distribution function, where an identical structure of local coordination environment was observed for hydronium ions with eight and 16 $H_2O$ molecules loaded on zeolite.[88] Additional water molecules are prone to adsorb onto the silanol groups and/or act as the free water outside the zeolite channels. Apart from the above advances, there is a lack of experimental information for the structural and composition of water clusters formed in large pore-sized zeolites (*e.g.*, H-FAU) and other microporous materials. The question arises as to what is the stable composition of water clusters in the presence of adsorbates such as alcohols and bases of various strength that can potentially replace water molecules in the zeolite pores. Moreover, the structure of water clusters remains unclear under realistic reaction conditions, since zeolitic materials are catalytically applied at higher pressure and temperature. It will be thus essential for future studies to evaluate above aspects related to the water structures on zeolite surface.

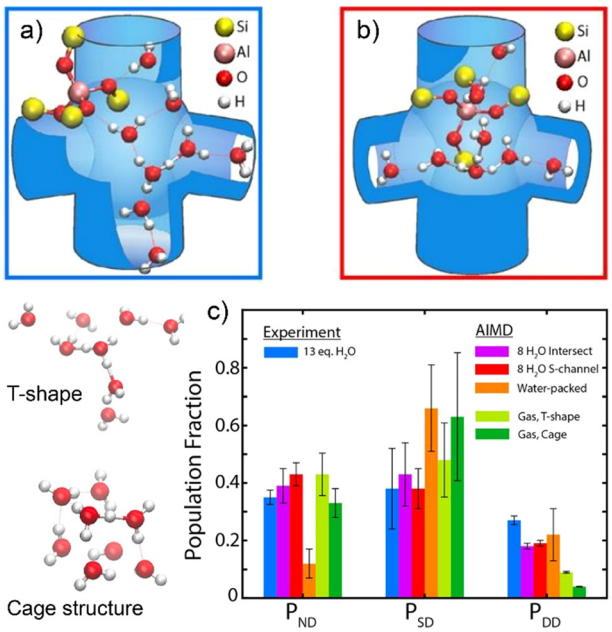


Fig. 3 AIMD simulation of the configuration of protonated water cluster in (a) the straight channel and (b) the intersection with zigzag channel of H-ZSM-5. (c) Comparisons of the distributions of ND, SD, and DD water molecules between IR spectra fitting and AIMD simulations. The models of gas-phase water clusters with T-shape and cage configuration are presented on the left side of plot. Reproduced with permission from ref. 100. Copyright 2021, American Chemical Society.

The molecular structure and H-bonding configuration of water clusters in protonic zeolite was recently studied by Hack *et al.*,[100] enabled by collecting 2D IR spectra and AIMD simulations using DFT at the revPBE/DZVP level of theory. Water clusters with a composition of $H^+(H_2O)_8$ are simulated to have branched configurations composed of a Y-shaped cluster at the channel intersections and an elongated configuration inside the straight channels (Fig. 3a and b). For a $H^+(H_2O)_8$ water cluster occluded in H-ZSM-5 zeolite, water molecules those donate two H-bonds (DD), donate one single H-bond while one free O–H bond (SD), and those donate no H-bonds (ND) are considered and quantified from the AIMD simulations. Results indicate that zeolite intersections are capable of accommodating a high degree of connectivity and the water molecules adsorbed in channel intersections possess a slightly larger fraction of SD, whereas those in the straight channel bring out a greater fraction of ND (Fig. 3c). The tight confinement effect in zeolite pores make the fractions of the H-bonding of water molecules in $H^+(H_2O)_8$ water clusters completely different to those of gas-phase protonated water clusters that manifest the T-shape and cage structures as the stable configurations (Fig. 3). The authors anticipated that these findings could enhance the understanding of zeolite hydration behaviors under hydrous conditions and the mechanistic descriptions of zeolite acid chemistry.

### 2.2. Lewis acidic zeolites

The structure of the BAS site on aluminosilicate zeolites has been well defined as the bridging Si(OH)Al unit.[40] Comparatively, the generation and the structures of Lewis acid sites

 

(LAS) related to the Lewis acidic aluminum have remained not well-understood.[101–103] This originates from the dependencies on the zeolite framework, Si/Al ratios, hydrothermal synthetic and postsynthetic procedures (calcination, steaming, acid leaching, and so on), exposure to varied conditions (in the dehydrated or hydrated form) and practical catalytic reaction conditions. In general, the aluminum ions with three-coordinated, tetrahedral, penta-coordinated and octahedral coordination environment are the potential precursor species for the formation of Lewis acidic sites in zeolite structures.[102–108] Lewis acidic aluminum sites on the aluminosilicates can be originated from framework, framework-associated or extra-framework species. It calls for detailed structural understandings about these sites by employing various instrumental techniques, *e.g.*, MAS NMR.[103–105] In addition, a reversible switch between tetrahedral and octahedral coordination exists for the framework-associated aluminum sites.[101,102] Assigning Lewis acid sites to the extra-framework aluminum debris and further correlating to Lewis acidic property of a zeolite do not hold in most studies.[101] Exchanging of a portion of framework $Si^{4+}$ with tetravalent atoms, such as $Ti^{4+}$, $Sn^{4+}$ and $Hf^{4+}$ could result in discrete Lewis acid sites and unique hydrophilic/hydrophobic properties of zeolite.[109,110] Lewis acidic zeolites can serve as the active and selective acidic catalysts for alkene epoxidation,[111] sugar isomerization,[112–115] alcohol dehydration,[116,117] Baeyer–Villiger oxidation[118] and many other reactions.[119,120] In addition to be a solvent for catalytic reactions, water may possess the opportunity of contacting (or binding) with zeolites upon calcination and subsequent exposure to ambient air or under post-synthetic conditions (*e.g.*, ion-exchange treatment). On Lewis acidic zeolites, the adsorption of water mainly occurs on the isolated heteroatom substitutions and silanol groups or framework defects in the pores. Detailed understanding of the interactions of water with certain types of Lewis acidic zeolites is pivotal as well to performing catalytic transformations with optimal efficiency.

**2.2.1. The interactions of water molecules with framework heteroatoms.** Due to the relevance of water in catalytic transformation reactions on Lewis acidic zeolites, the structural coordination of active sites (*i.e.*, heteroatoms) upon water adsorption has been investigated with the aim of understanding the reaction mechanisms. It was found that the interactions between water and tin (Sn) sites are more exothermic than with titanium (Ti) sites, suggesting a higher Lewis acidity and hydrophilic nature of Sn-BEA than Ti-BEA and purely siliceous zeolites.[121,122] One water molecule was characterized to be coordinated with each titanium atom in defect-free Ti-BEA and titanium silicalite-1 zeolite, resulting in a coordination number of six for the titanium site.[121,123] In addition, for the hydrophobic Sn-BEA material synthesized under a fluoride anion condition, Gounder *et al.*[113] identified that each framework tin center coordinates with two water molecules. This was verified by transition of the coordination configuration of tin site from octahedral to tetrahedral after measuring $^{119}$Sn MAS NMR spectra under the hydration and dehydration states. Similarly, the $Sn^{IV}$ sites in zeolite Sn-BEA with six-fold coordination were identified to act as one of the two type of active sites by solid state NMR and DFT calculations.[124] According to the X-ray absorption spectroscopy measurements and theoretical calculations, a stoichiometric water coordination of *ca.* two per the metal center on the hydrophilic and hydrophobic Ti-Beta and Sn-Beta zeolites was also suggested.[121,125,126] It should be noticed that water adsorption can cause the partial hydrolysis of framework centers and further make a difference on the nature of active sites, as in the case of the partial hydrolysis of tin atoms on Sn-substituted BEA zeolite by forming open site $Sn(OSi)_3OH$.[114] Framework partial hydrolysis also makes the zeolite pores hydrophilic due to the formation of Si–OH species and facilitates the formation of water structures inside of the Lewis acidic zeolite pores, eventually giving rise to structural changes and stability degradation, which will be discussed in Section 4.

The composition of water structures stabilized on Lewis acid sites can be determined by gaseous water uptakes.[127,128] For example, Bregante *et al.*[128] reported that each framework titanium atom with a structure of $Ti(OSi)_4$ in Lewis acidic Ti-substituted MFI zeolites was able to stabilize about five water molecules at the saturation pressure of water at 293 K. Si-MFI zeolite was measured under a similar condition to subtract the contribution of water adsorption on silanol nest defects. Since the chemical potential of water adsorbed at the titanium site equals that of saturated water in gas phase and even that of water in bulk aqueous phase, the number of water adsorbed on the Ti-MFI zeolite reflects the size of water clusters when engulfed in condensed water. Interestingly, niobium (Nb)- and tantalum (Ta)-substituted MFI zeolites were characterized to contain weak BAS in this work.[128] Each framework niobium and tantalum stabilized seven to eight water molecules upon the saturated adsorption of water molecules, showing the similarities with the size of water clusters that are formed on the aluminum-containing Brønsted acidic zeolites (except for H-BEA[97]) in gas or liquid water phase.[88,95,98–100]

**2.2.2. The interactions of water molecules with surface defect sites.** Comparing with the framework heteroatom substitutions, surface defects in the pores are more characteristically hydrophilic and thus are capable of nucleating water molecules in the pores of Lewis acidic zeolites.[110,122,128–130] DFT calculations on the hydrolyzed tin sites of Sn-BEA zeolite have revealed that water clusters were tightly bound to Sn–OH and Si–OH at four to six water per unit cell, whereas silanol nest defects could promote the stabilization of delocalized mobile water networks.[122] The hydrophilic binding sites on Lewis acidic zeolites can be quantified by measuring IR spectra after saturation of zeolite with $CD_3CN$ at 303 K, where a critical threshold for the defect sites needed to stabilize the extended water networks was speculated.[129] Herein, hydrophobic Sn-Beta sample containing $<1$ defect per unit cell only allows the local nucleation of water clusters in the micropores, whereas extended hydrogen-bonded water networks could be formed and fully stabilized in the pores of hydrophilic Sn-Beta zeolites comprising higher densities ($>1$ per unit cell) of defects. Above

works indicate that the formation and structural properties of water structures inside of the pores are reliant on the hydrophilicity/hydrophobicity (or the densities of defect sites) of Lewis acidic zeolites.

Difference in the densities of defect sites could cause an obvious variation in the water uptakes inside of the pores. In the work of Cordon *et al.*,[125] at the partial pressure ($P/P_0$) between 0 and 0.2, about 20–25 times higher water uptakes were measured on hydrophilic Ti-Beta zeolites synthesized in a $OH^-$ condition than on hydrophobic Ti-Beta zeolites that were prepared in fluorine media. Hydrogen-bonded water networks are prone to form on hydrophilic Ti-Beta zeolites with increasing of water chemical potential, as indicated by the full perturbation of hydroxyl groups from the IR spectra upon water adsorption. Bregante *et al.*[128] reported that the density of surface silanol groups on Lewis acidic MFI zeolite varied with the ratio of hydrofluoric acid (HF) to structure-directing agent (tetrapropylammonium hydroxide, SDA) in the process of hydrothermal synthesis. The MFI zeolite synthesized with a HF/SDA ratio of 1.5 was determined to possess a water uptake 100 times less than that of the analogous material prepared in the $OH^-$ condition (*i.e.*, zero HF-to-SDA ratio).

**2.2.3. Structural characterizations of the water structures on Lewis acidic zeolites.** Water structures within series of Ti-substituted Lewis acidic zeolites (with low loadings of titanium) have been quantitatively investigated by the means of *in situ* IR

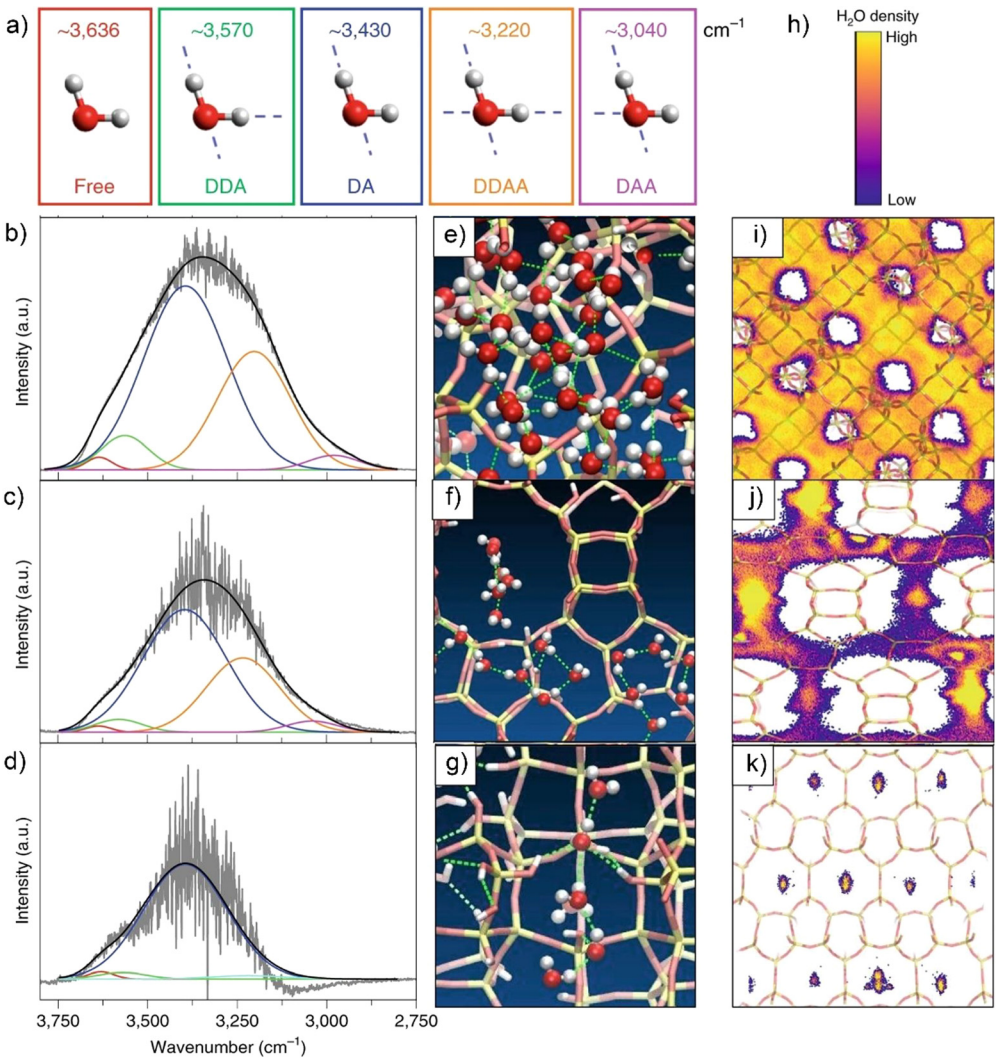


Fig. 4 (a) Spectroscopically observed H-bonding configuration of $H_2O$ (Details for the abbreviations: ''free'' means water molecules are lack of hydrogen-bonding (HB); DDA: water donates two and accepts one HB; DA: water donates one and accepts one HB; DDAA: water donates two and accepts two HBs; DAA: water donates one and accepts two HBs). IR spectra of $H_2O$ over a ZnSe internal reflection element within the pores of Ti-FAU-OH (b), Ti-BEA-OH (c) and Si-CDO-OH (d). Snapshot of MD simulations of $H_2O$ in the pores of Ti-FAU-OH (e), Ti-BEA-OH (f) and Si-CDO-OH (h) constructed with five $Si(OH)_4$ per unit cell. The dashed lines denote as the H-bonding between $H_2O$ molecules. Time-averaged spatial distributions of $H_2O$ after 1 μs MD simulation projected onto 2D images of Ti-FAU-OH (i), Ti-BEA-OH (j) and Si-CDO-OH (k). (h) The heat map bar for water spatial distributions with low (purple) to high (yellow) densities. The experiments of collecting IR spectra and MD simulations are all conducted at 313 K. Reproduced with permission from ref. 126. Copyright 2021, Springer Nature.

 

spectroscopy and molecular dynamics (MD) simulations in a recent work of Bregante *et al.*[126] Zeolite materials with different pore topologies (*e.g.*, FAU, BEA, MFI, CDO) and polarities were involved in this study. From the vibrational spectra of Ti-FAU, water molecules in the 1.3 nm supercages are indicated to form 3D bulk-like structures with spatial freedom (Fig. 4b, e and i), showing the dominant DDAA bonding configuration (water that both donates and accepts two hydrogen bonds). In contrast, water molecules confined in the narrow pore zeolites, *e.g.*, Ti-BEA, Ti-MFI and Si-CDO, possess a large fraction of DA configuration (water that donates one and accepts one hydrogen bond) (Fig. 4c, d, f and g). DDAA configurations also exist at the intersections of Ti-BEA and Ti-MFI zeolites with both hydrophilic and hydrophobic properties.

In above work, as calculated from the IR vibrational spectra and MD simulations, the average number of hydrogen bonds decrease with the decreasing of pore dimensions.[126] Comparing to Ti-FAU-OH, the hydrophilic Ti-BEA-OH, Ti-MFI-OH and Si-CDO-OH zeolites possess a gradually increased and higher percentage of hydrogen bonds that are formed between water and silanol defects. These lead the authors to state that water molecules in zeolite BEA, MFI, and CDO pores coalesce into one-dimensional oligomers/chains, which are different from that fabricated in the FAU pores (Fig. 4e–k). Of note, forming hydrogen bonds confer the stability to the water structures in larger pores, but these water structures are susceptible to lose stability with decreasing the pore diameter from 1.3 to 0.45 nm. These pore-size-dependent water structures have to reorganize themselves through breaking hydrogen bonds to enable surface catalysis and alter the free energy landscape of catalysis at the solid–liquid interfaces (*vide infra*).

# 3. Roles of water structures in zeolite catalysis

## 3.1. Tailoring the chemical thermodynamics of reactive substrates and intermediates on the surface

Catalytic reactions on acidic zeolites usually involve an initial adsorption of reactant molecules into the pores and a subsequent interaction (*e.g.*, H-bonding or protonation) with the surface acidic sites (*e.g.*, BAS, LAS), before the intrinsic activation step. Zeolite pores can stabilize gaseous reactant molecules through van der Waals forces that depend on the size of pores and the diameter of reactant molecules. In contrast, in liquid-filled pores of zeolites the thermodynamics of liquid-phase reactions can be greatly altered by the solvent molecules (*e.g.*, water). The thermodynamic terms mainly cover the energies of sorption, solvation and interactions of reactants or between reactant and surroundings.[16] The adsorption behaviors of reactant molecules on Brønsted and Lewis acidic zeolites from anhydrous and hydrous gas phase and aqueous liquid phase are illustrated in Scheme 1. Typical effects of water structures on the thermodynamics for reactant molecules and surface intermediates on zeolites are discussed as follows.

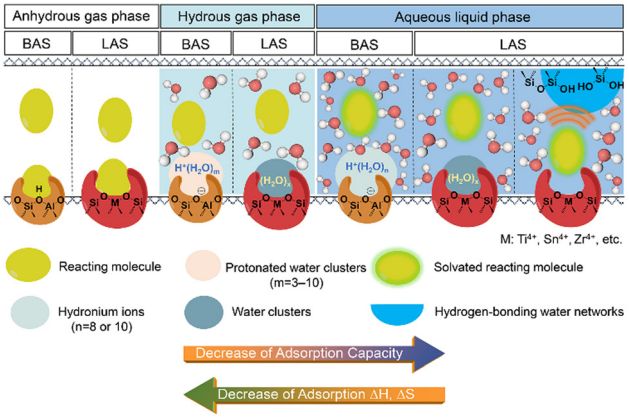


Scheme 1 The illustrations of the adsorption of reactant molecule on the BAS and LAS sites of zeolite in anhydrous and hydrous gas phase and aqueous liquid phase.

**3.1.1. At the solid–gas interfaces.** Water molecules at the solid–gas interfaces can directly modulate the coverage of active sites through competitive adsorption, which is accompanied by the limited amount of unoccupied sites for substrate molecules that subsequently deteriorate to the catalytic reactions on solid zeolite catalysts.[9,17,131–134] For example, water competes with ethene for the access to the BAS by displacing the adsorbed ethene molecules in H-ZSM-5 pores. It causes a low intrazeolite concentration of ethene and a serious suppression for the oligomerization reaction of ethene on zeolite catalysts.[132,133] As observed by De Wispelaere *et al.*,[134] co-feeding water with methanol stream in methanol-to-olefins (MTO) process reduced the availability of acidic sites for methanol and primary product, *i.e.*, propene *via* the competitive adsorption phenomena. In this case, MD simulations at the revPBE-D level of theory revealed that increasing of water amount in the CHA cage of H-SAPO-34 zeolite could lower the possibility of the activation of propene, and delay the formation of aromatic hydrocarbon pool species, ultimately leading to a longer induction period for the MTO conversion.

Competitive adsorption between co-feeding water molecules and coke precursors has been positively applied to depress coke formation in the MTO process.[135–137] The consequences in terms of either eliminating catalytic reactivity or quenching the deactivation of zeolites are reliant on the concentration of co-fed water in the reactant stream.[135] In addition, for the conversion of methanol with dimethyl ether to produce propylene on H-ZSM-5 zeolite, water in the stream was found to facilitate olefins desorption and ultimately allow for obtaining the desired product distribution.[138] The competition-induced desorption by water was also used to explain the achieved high selectivity of linear alkanes from *n*-hexadecane hydrocracking process on a Pt-containing shape-selective MFI catalyst.[139] In this case, water at the MFI acid sites effectively minimized the probability of the secondary cracking and isomerization of the primary cracking products, achieving 80% selectivity of linear cracking products at 80% n-$C_{16}$ conversion at a low temperature (225–235 °C) and high space times

(3500–28 000 kg s mol$^{-1}$). Note that a large portion of water molecules adsorbed on the BAS sites are prone to desorb with decreased equilibrium pressure and at elevated temperatures, which might be accompanied by the diminished concentration of hydrogen-bonded complexes and protonated water clusters in the zeolite pores.[50,53,132] That is, water competitive adsorption phenomena may become less pronounced when operating a catalytic reaction under high-temperature conditions.[45,133,140] It has been shown to be the case for ethene to aromatics reaction on H-ZSM-5 zeolite when operating the reaction at above 300 °C, where the deterioration effects of water in terms of suppressing the conversion of ethene, the yield of aromatics and hydrogen transfer process, and changing product distributions became relatively insignificant.[133]

Water molecules also participate in the formation or transformation of reactive intermediates on the surface of acidic zeolites. For example, co-feeding of water was found to shift the equilibrium constant of formaldehyde hydrolysis, which can result in a low concentration of formaldehyde and the reduced initiation and termination rates during the MTO conversion on H-SSZ-13 zeolite.[141] Such mechanistic role of water is responsible for the long induction period and high total turnovers observed for MTO with water cofeeds. Not limited to water, note that some reactant molecules such as low-carbon chain alcohols (*e.g.*, methanol, ethanol) can be protonated by the BAS of zeolites.[142] Water-reactant-clusters such as $(C_2H_5OH)(H^+)(H_2O)_n$ cluster have been identified on H-BEA zeolite for the gas-phase ethanol dehydration at a low water pressure ($<$ 10 kPa).[96] In addition, water-ethanol dimers (co-existed with the reactive ethanol–ethanol dimers) have been observed on Sn-BEA zeolites and their coverages on the surface depend on the polarity of zeolite pore environment.[116] The formation of water-reactant-clusters usually leads to inhibitory effect on zeolite catalysis.

**3.1.2. At the solid–liquid interfaces.** Zeolite intraporous solvating environment involving the specific interactions with a condensed water phase make the thermodynamics of catalytic reactions complex. Linear correlations between adsorption enthalpies of reactant/intermediate and measured apparent activation energies often exist for liquid phase catalytic reactions.[143] It is essential to investigate how the intraporous water structures affect the thermodynamics and kinetics of zeolite catalysis. The energetic contributions for reactant adsorption enthalpy can be deconvoluted into reactant desolvation enthalpy ($\Delta H_{R,solvation}$), enthalpy changes ($\Delta H_{\Delta solv}$) for water molecules in bulk phase and in zeolite pores, disrupted by gaseous reactant molecule adsorption into the zeolite pore, interaction energies ($\Delta H_{R\text{-}zeo} + \Delta H_{R\text{-}solv}$) between adsorbed reactant and zeolite pores/water molecules, as illustrated from the thermodynamic cycle in Scheme 2. Given that water interactions also bring about entropic effect on chemical thermodynamics, a similar scheme based on Gibbs free energies can be drawn. Each energetic contribution can be estimated by performing experimental measurements or computational modelling.

As for Brønsted acidic zeolites, hydrated hydronium ions are inclined to occupy the hydrophilic volume space of micropores,

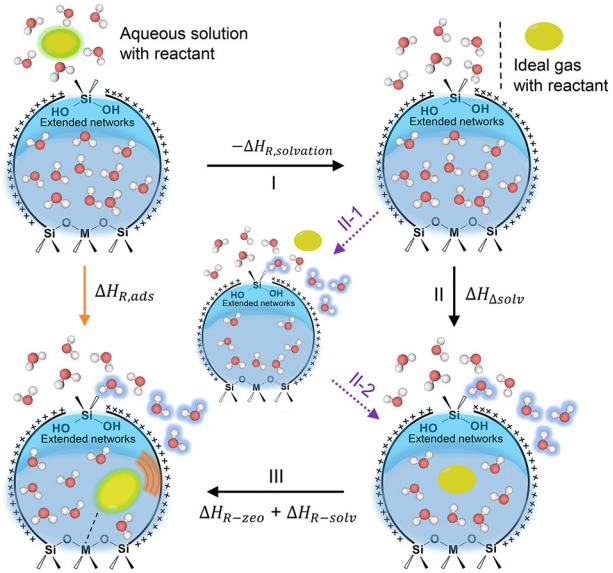


Scheme 2 Thermochemical cycle for the deconvoluting enthalpic contributions of $\Delta H_{R,ads}$. Herein, Lewis acidic zeolite pore with heteroatom substitutions (M: Ti, Sn, Zr, *etc.*) and silanol defect sites on the internal surface is taken as the example. I step: formation of ideal gas reactant molecule from aqueous solution; II step: reactant molecule adsorbs into solvent-filled zeolite pore from gas phase, accompanied by the displacement of inside water molecules (further illustrated by dashed purple arrows in this scheme); III step: adsorbed reactant molecule interacts with water structures and zeolite pores.

showing a strong dependency on the concentration of framework aluminum sites.[95] Fig. 5a shows that organic molecules preferentially adsorb into the hydrophobic volume space that are preserved to be unoccupied by the hydronium ions in H-MFI channels/cavities. The distance between the center of hydrated hydronium ion and the center of nonpolar domains ($d_{h\text{-}n}$) sharply decreases with the increasing amount of the BAS (that is decreasing of Si/Al ratios) (Fig. 5b). Consequently, the adsorption uptake of organic molecules into the hydrophobic volume from the aqueous phase are decreased.[144] On the other hand, zeolite-confined hydronium ions provide a ''quasi solid electrolyte'' environment and thereby a specific ionic strength in the pores.[95] The values of ionic strength determined by normalizing the concentration of BAS to the micropore volume of H-MFI display a proportional relationship to the BAS concentration.[95,97] A high ionic strength does in turn dictate the chemical potential of sorbed cyclohexanol and its stabilization state as well. A trend observed for cyclohexanol adsorption on H-MFI illustrates that the chemical potential of cyclohexanol ($\mu^+$) increase with the decrease of distance between the center of polar and nonpolar domains ($d_{h\text{-}n}$) (Fig. 5b). This trend indicates the stronger destabilization of cyclohexanol caused by the presence of confined hydronium ions in zeolite pores. The typical exhibition of destabilization effect is the smaller adsorption heat and adsorption constant in an aqueous phase. As a result, the interactions of the organic part of reactant with zeolite are weakened and the corresponding interactions with the protons are favored in the

 

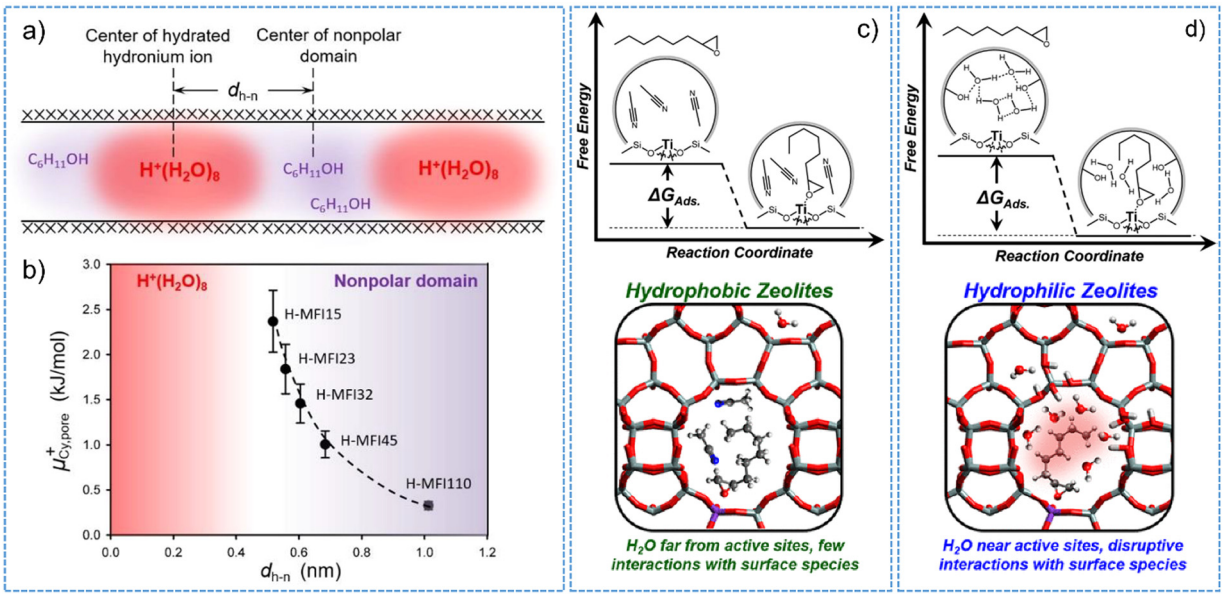


Fig. 5 (a) Schematic illustration of hydronium ions and nonpolar domain in H-MFI channels. (b) Chemical potential of cyclohexanol adsorbed in zeolite pores as a function of $d_{h\text{-}n}$. The $d_{h\text{-}n}$ is the distance between the center of polar and nonpolar domains. Reproduced with permission from ref. 95. Copyright 2019, Wiley-VCH. Free energy profile (upper) and schematic illustrations (bottom) for the adsorption of $C_8H_{16}O$ (1,2-epoxyoctane) in hydrophobic (c) and hydrophilic (d) pores of Ti-BEA. Reproduced with permission from ref. 143. Copyright 2019, American Chemical Society.

non-ideal system with distinct ionic strength. Recently, different extent of the destabilization effect on reactant molecules was observed by comparative studies on the hydronium ions confined within the pores of H-ZSM-5 and H-BEA zeolites.[97] A slight increase in the size of hydronium ions (*i.e.*, from $H^+(H_2O)_8$ to $H^+(H_2O)_{10}$) could cause obvious differences on the calculated excess chemical potentials of the sorbed substrate (*i.e.*, 0.3–2.4 kJ mol$^{-1}$ for H-ZSM-5 *vs.* 0.1–1.8 kJ mol$^{-1}$ for H-BEA).

The thermodynamics of adsorption in acidic zeolite micropores with the presence of different solvent including water have been studied by employing pyridine, a typical base probe molecule.[145,146] Owing to the efficient stabilization effect of water solvation on the protons of BAS, desorption of protonated pyridine from H-ZSM-5 pores shifted to occur at lower temperature, comparing to the system with liquid acetonitrile, n-heptane or to that upon exposure to a vacuum condition.[145] The adsorption enthalpy and entropy of pyridine molecules on H-ZSM-5 in the aqueous phase were lower in magnitude than those measured from the gas phase.[146] A low enthalpy value was the typical consequence of the intermolecular interactions between adsorbate and water molecules, and the displacement of water molecules occluded in zeolite pores upon the adsorption of substrate molecules from water phase. The less-extreme value of adsorption entropy was associated to the restrictions by zeolite confinement effect on the translational/rotational degrees of freedom. In addition, compared to mesoporous materials (*e.g.*, MCM-41 and SBA-15), the formation of Brønsted acid site-pyridine interactions could be facilitated on H-ZSM-5 and H-BEA zeolite, showing typical Langmuir characters for the measured pyridine adsorption isotherms in water atmosphere.[146] These works additionally point to the importance of an elaborate choice of solvent and the potential effects of solvent on the catalytic reactions performed in condensed aqueous phase.

The hydrogen-bonded water clusters on Lewis acidic zeolite can also impact the reactant adsorption thermodynamics and subsequent catalysis processes.[110,143] In addition to the dependency of adsorption capability on the zeolite chemical functionality, the formation of stable surface intermediates following the reactant adsorption and molecular interactions with intrazeolite water clusters should be crucially considered.[126,130,143] An example for this is the Lewis acidic Ti-BEA zeolite, on which the hydrogen-bonded water molecules stabilized by silanol nests (*i.e.*, $[Si(OH)]_4$) must reorganize to accommodate the surface intermediates that are adsorbed on the active sites (Fig. 5c and d).[143] The consequence is that the values of adsorption enthalpy and entropy for $C_8H_{16}O$ (1,2-epoxyoctane) were observed to be 19 kJ mol$^{-1}$ and 75 J mol$^{-1}$ K$^{-1}$ more-positive on Ti-BEA with five silanol groups per unit cell than those determined from the defect-free hydrophobic Ti-BEA sample. Such differences are negligible for the Ti-BEA zeolite measured with the absence of water in an acetonitrile solvent. The free energies of adsorption typically reflect the restructuring of water molecules nearby the framework Ti active sites and lean on the specific interactions at the solid–liquid interfaces, which can be described as excess free energy contributions. A linear free energy relationship between the adsorption and transition state for 1-octene epoxidation reaction suggests the crucial role of surface chemistry involving water structures in impacting the stability of surface adsorbed intermediates and altering the chemical thermodynamics at

the solid–liquid interfaces.[126] More recently, using alkene epoxidation reactions on Ti-BEA zeolites in liquid solvent, Potts *et al.*[130] have investigated the kinetic and thermodynamic consequences of the specific interactions in solvent-filled pores and revealed the origins of these interactions. The requisite reorganization of solvent molecules (*e.g.*, $CH_3CN$, water, or $CH_3CN$–water mixture) inside of the pores of zeolite Ti-BEA allows the adsorption and suitable accommodation of alkene molecules with different carbon chains. The amount of solvent molecules displaced from zeolite pores determines the stability of adsorbed intermediates, thereby influencing rates and selectivity of catalytic reaction.

### 3.2. Impacting the catalytic reactivity of surface catalysis on zeolite

Ways of tailoring the reactivity of zeolite catalysis by water structures can be diverse, which have been depicted in Scheme 3. Competitive adsorption phenomena exists in both gas phase and aqueous phase for determining the accessibility of reactant molecules to active sites in the pores of zeolites. Water structures on Brønsted and Lewis acidic zeolites can actively participate in the formation of surface intermediates, induce the stabilization/destabilization of reacting intermediates and transition states, thereby modifying the activation Gibbs free energies for a catalytic reaction. In addition, the changes in the nature of active sites and zeolite pore structural properties in the presence of water are also responsible for the structure–performance relations of zeolite catalysis.

**3.2.1. Decisive roles of water loading and zeolite pore polarity.** Manipulations of the reactivity of zeolite catalysis are most often dependent on the properties of water structures and the reaction conditions of interest.[140,147–149] Chen *et al.*[147] reported that a *ca.* $\leq 1$ water molecule per the BAS on H-ZSM-5 benefited a factor of 10 for the increase in the reaction rate

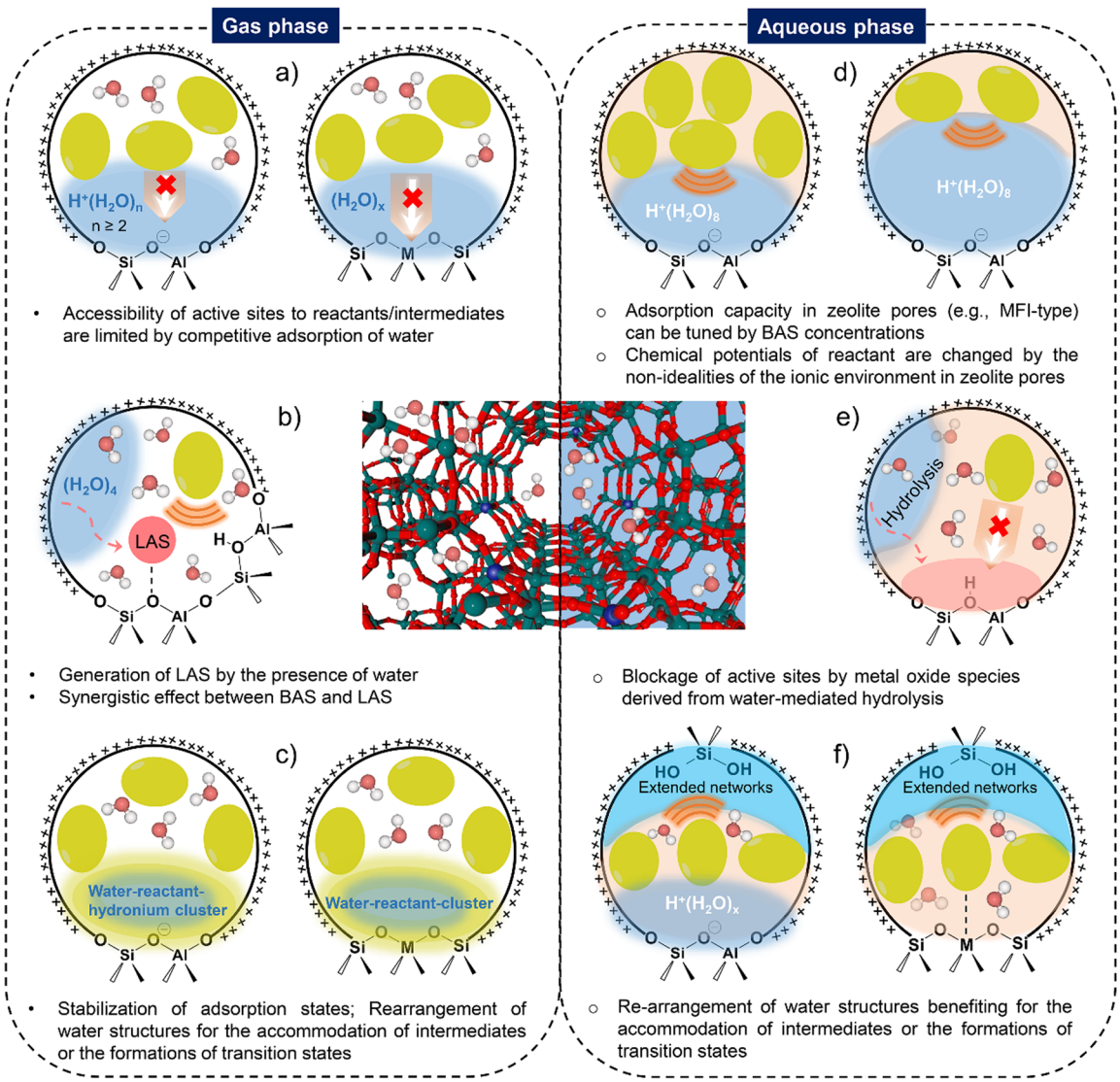


Scheme 3 The illustrations of the different ways by water structures for manipulating the zeolite-catalyzed reactions in hydrous gas and in aqueous phase.

 

constant for isobutane cracking reaction at room temperature. Trace water also increased the benzene H/D exchange rate on H-ZSM-5; the lower the Si/Al ratio becomes, the higher the reinforcement degree gets.[148] Sub-stoichiometric amount of water actively participate in the catalytic reactions probably *via* the stabilization of transition state, as suggested by *in situ* solid-state NMR data. Under the condition involving more than two adsorbed water molecules per the active site (*i.e.*, BAS), however, these reactions all display suppressed catalytic activities, owing to the loss of active sites in the presence of water clusters with a higher proton affinity than hydrocarbon molecules (Scheme 3a).[147,148] Very recently, Bocus *et al.*[149] have studied the chemical effects of water in the *para*-protonation of ethylbenzene product produced from benzene ethylation reaction with ethene or ethanol on H-ZSM-5 zeolite. Water actively acts as proton-transfer agent in the system containing one water molecule per BAS, resulting in one order of magnitude of increase in the catalytic reaction kinetics. Namely, water tends to facilitate the formation of Wheland intermediate (protonated arenium ion) *via* both the stepwise and concerted mechanism in zeolite pores and hence accelerate the acid-catalyzed alkylation reactions of aromatic substrates. Increasing water loadings (that is more than three water molecules per the BAS) could induce the solvation of active sites to strongly stabilize the reactant state and thus cause a decreased protonation rate of ethylbenzene. Since water can heterogeneously distribute within zeolite pores after forming the cation-ion pairs by the protonation of BAS site,[68] the authors claimed that the boost in activity is unlikely to be measurable when the coverage is one water per the BAS.[149] Nevertheless, it is regarded as important to study the role of water in the catalytic reactions, in which water is generated as a stoichiometric byproduct, such as the MTO conversion and alcohol dehydration catalyzed by acidic zeolite materials.

Water inhibitions have been intensively observed for gas-phase alcohol dehydration on acidic zeolites (Scheme 3c).[96,116,150] For example, at low water pressure (<10 kPa), a −1 order dependence on the water pressure for the ethanol dehydration was measured. It was the consequence of the need to displace one water molecule in the $(C_2H_5OH)(H^+)(H_2O)_n$ cluster by ethanol on the acid sites of H-BEA.[96] Increasing of water pressure led to the formation of $(C_2H_5OH)(H^+)(H_2O)_{4-5}$ with the maximum water–ethanol cluster size and the additional water molecules tended to be hydrogen-bonded in zeolite microporous voids by solvating the water-ethanol clusters. Severe water inhibition with up to −3 of reaction order with respect to the water pressures (10–75 kPa) was ascribed to the more extensive disruption of hydrogen bonds involved at the transition states along the reaction coordinates. Furthermore, in the work of Zhi *et al.*[150] for the catalytic propanol dehydration on H-MFI catalyst, water molecules strongly and preferentially stabilize the ground state of propanol molecules prior to the transition state by forming protonated propanol-water dimer in the zeolite micropores, which results in a high activation barrier and thereby a decrease in the reaction rate. DFT simulations on propanol adsorption on BAS site with the presence of water molecules further suggested that water enhanced propanol adsorption (adsorption energies increased from −151 kJ mol$^{-1}$ for the case of without water to −163 kJ mol$^{-1}$ with two water molecules and −188 kJ mol$^{-1}$ with the presence of four water molecules) through hydrogen bonding.[81] The stability of propanol adsorption can be enhanced by forming protonated dimeric propanol and propanol-water complexes. These findings indicate that the formation of water-reactant-clusters on zeolites is detrimental to the catalytic events at the solid–gas interfaces with the presence of gaseous water.

More importantly, the polarity of confining environment of zeolite determines the extent of water inhibition and the catalytic rates for a chemical reaction. Specifically, the coverage of inhibitory ethanol–water dimers was found sensitive to the silanol defects on polar Sn-Beta-OH and non-polar Sn-Beta-F zeolites in the process of gas-phase bimolecular ethanol dehydration.[116] The equilibrium constant for the formation of ethanol–water and ethanol–ethanol dimer species on Sn-Beta-OH were determined to be three to four times higher than that in the case of Sn-Beta-F. However, similar kinetic rate constants were obtained for the employed Sn-Beta zeolites, irrespective of whether a highly polar or a less polar framework was involved. It was concluded that ethanol dehydration catalysis responds to the coverage of most abundant reactive intermediate, showing a sensitivity to the H-bonding interactions in zeolite confining nano-environments.[116] This work may provide a potential way to circumvent the issue of water inhibition on the catalytic reactivity of zeolite catalysis.

In addition to the inhibitive consequences on zeolite activities, the effect of water on zeolite-catalyzed reaction can become positive. Gešvandtnerová *et al.*[151] observed that water molecules generated from catalytic reaction could mediate proton transfer processes and strongly stabilize the π-complexes of alkenes when performing DFT calculations to explore the monomolecular mechanism of isobutanol conversion to butenes on acidic chabazite zeolite. In another typical work of Chau *et al.*,[152] enhanced rates were observed for cumene dealkylation on H-ZSM-5 zeolites upon water co-feeding. Upon water adsorption, protons from the framework can be delocalized in the form of hydronium ion clusters and the interactions between cumene and hydronium ion clusters were proposed to result in a reaction transition state with more degrees of freedom and thus a less negative activation entropy, comparing to the condition without the presence of water. This work highlights the necessity of exploring and understanding the roles of water on catalytic transformations of different hydrocarbon molecules. Above cases show that the active participation of water in catalytic reactions can be reflected by the formation/stabilization of surface intermediates and transition states, thus influencing the catalytic rates on zeolitic materials.[96,116,148–152]

Moreover, the positive effect of water on gas-phase catalytic reactions can be resulted from manipulating the diffusivity of reactive compounds and products around the acidic active sites in zeolite pores. Based on solid-state NMR measurements and theoretical simulations, Wang *et al.*[153] have recently demonstrated that water clusters generated on the BAS could promote

the diffusion of benzene molecules in zeolite channels and drive their interactions with surface methoxy species (SMS) to obtain highly active SMS-Benzene complexes, eventually improving the methylation reactions of benzene with methanol. This work provides the atomic- and molecular-level insights on the micro-hydrophobic effect induced by water in confined zeolite-catalyzed reactions. In addition, performing DFT simulations to study the reactivity of zeolite-catalyzed alkylphenol dealkylation reaction at high temperatures, Bocus *et al.*[154] found that the competitive adsorption of water molecules with phenol products on the BAS sites could benefit a short residence time of phenol, which further prevents both the poisoning of active sites and catalytic deactivation from being taken place. Although there are some statement in the literatures that the interactions of water molecules with zeolite internal surface could affect the diffusion of reactants/products and further the reaction kinetics,[18,39] this effect is relatively unexplored and in-depth studies are still desired.

Similar to the scenario at the solid–gas interfaces, water clusters and/or extended hydrogen-bonded water networks in zeolite-confined micropores dictate the sorption behavior of reacting molecules from aqueous solution and the formation/stabilization of active surface intermediates and transition states (Scheme 3d and f), eventually leading to differences for catalytic performance.[114,144] For example, higher turnover rate for phenol alkylation reaction with ethanol in an aqueous phase was measured on H-MFI zeolite that possesses a low amount of hydronium ions (*i.e.*, a high Si/Al ratio) in the micropores.[144] The competition between hydronium ion clusters and phenol molecules for the adsorption sites on zeolite imposed no effects for the intrinsic rate constant and product selectivity. It is increase in the adsorption capability of phenol in zeolite H-MFI pores that contributes to the observed enhanced alkylation rates. In analogy to above case, a decreased accessibility of framework Lewis centers to reactant molecules in Sn-Beta and Ti-Beta zeolite pores is responsible for the decrease in the rate of sugar isomerization in aqueous phase.[113,155] In the work of zeolite-catalyzed dehydration of polyalcohols and ethylene-vinyl alcohol copolymer in γ-valerolactone (GVL) polar aprotic solvent, the strong adsorption of GVL on framework BASs was found to mitigate the surface coverage of reacting intermediate and cause reduced dehydration rates.[156] Interestingly, the addition of water into GVL solvent could tackle the competition of reacting intermediate with GVL molecules for active sites and improve product formation rates. It was achieved by the delocalization of BAS sites from zeolite framework into hydronium ion clusters, the latter serve as mobile active sites. These works also demonstrate the integral role of optimal solvent for catalytic upgrading of biomass compounds and polymer wastes in liquid phase.

There are several scientific advances recently reported from the Lercher group on the topic of acid catalysis by hydronium ion clusters confined in Brønsted acidic zeolites with varied concentrations of BAS. Zeolite confinement effect can synergistically promote the association of reactant molecules with the confined hydronium ions in comparison to those interacted with un-confined hydronium ions in homogeneous acid solution, *e.g.*, phosphoric acid.[157–159] Specifically, the positive impacts of confinement effect in zeolite H-MFI on enhancing the reaction rate for aqueous-phase dehydration of cyclohexanol and secondary alkanols (*e.g.*, 3-heptanol and 2-methyl-3-hexanol) are ascribed to the enthalpic stabilization of transition states in the micropores, although less positive activation entropies were determined from the study of kinetic aspects.[158,159]

It is interesting to note that the hydrated hydronium ions in the micropores of high-crystalline H-MFI zeolite create a unique ionic environment, which eventually brings in non-ideality to a catalytic system.[95,99] The turnover frequencies (TOFs) of cyclohexanol dehydration at 423 K as a function of the BAS concentration were compiled into a volcano-shape plot (Fig. 6a), which firstly shows a six-fold increase of TOF values from the BAS concentration of 0.054 to 0.36 mmol $g^{-1}$ and then a 60% decrease at the BAS concentration of 0.86 mmol $g^{-1}$.[99] The non-ideality triggered by intraporous ionic environment leads to the deviations of activity coefficients from an ideal state, and thereby the excess chemical potentials of both adsorption ground state and transition states are determined. Positive values of the excess chemical potential for the ground state and the negative values of the excess chemical potential for the transition state contribute to the decreases in the activation barriers and, consequently, the increases in aqueous-phase cyclohexanol dehydration TOFs (Fig. 6b and c). Comparatively, in aqueous hydrochloric acid solution the rates for cyclohexanol dehydration increase monotonically with the ionic strength.

Similar catalytic function (changes of TOF values as a function of the BAS concentrations) was observed for the dehydration of substituted cyclohexanols in aqueous phase catalyzed by varied ionic environment in the H-MFI zeolites.[160] However, there were limitations in the rate enhancement for aqueous-phase alcohol dehydration in the ionic environment confined within microporous zeolite. The drop after a maximum position on the volcano plot was likely related to the size exclusion phenomena in the presence of high density of hydronium ions in the molecular-sized pores.[99] To be more specific, the adsorption of cyclohexanol molecule in the void space between the boundary of neighboring hydronium ion clusters can be markedly hindered when the void volume is smaller than the van der Waals volume of cyclohexanol ($\sim$0.2 $nm^3$ at 423 K). This thus leads to increased enthalpy of ground state and transition state and, in turn, the decreased TOF values (Fig. 6d). Through measuring the kinetics in the first-order regime to avoid substrate crowding influences, the size exclusion effects have been excluded for the aqueous-phase cyclohexanol dehydration on H-MFI zeolites.[161] It was concluded that the rate enhancement at high ionic strength can be partly compensated by the work to separate hydronium ion clusters and rearrange the cation–anion pairs within the zeolite pore network. Therefore, as demonstrated across the whole H-ZSM-5 zeolite crystals, intracrystalline ionic environments lead to a maximum in impact of ionic strength on acid-catalyzed reaction rates.

 

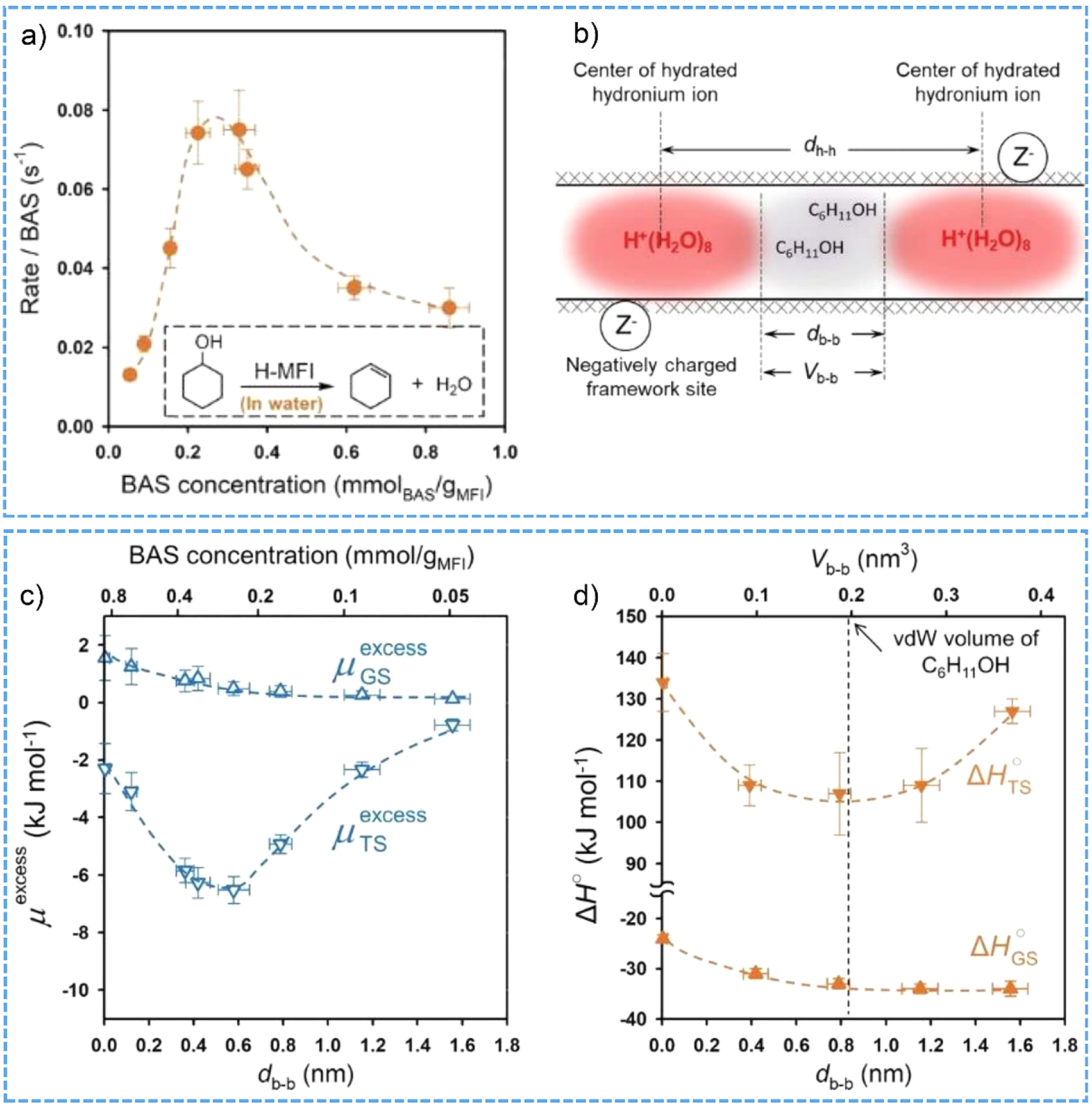


Fig. 6 (a) The BAS-normalized reaction rates for aqueous-phase cyclohexanol dehydration on H-MFI zeolites with varied concentration of BAS at 423 K. (b) Schematic illustrations of the mean distance $d_{h\text{-}h}$ between two neighboring hydronium ions, the mean distance $d_{h\text{-}h}$ and volume $V_{b\text{-}b}$ between the boundaries of hydronium ions in H-MFI pore. The calculated excess chemical potential (c) and enthalpy (d) of the ground (GS) and transition state (TS) as the function of $d_{b\text{-}b}$. Reproduced with permission from ref. 99. Copyright 2021, AAAS.

In analogy to the case of Brønsted acidic zeolites, water structures occluded inside of Lewis acidic zeolite pores alter the reactions of molecules by impacting the excess free energies for the transition states. Cordon *et al.* reported that, inside of the hydrophobic pores of Ti-Beta-F zeolite, the adsorption of glucose could promote the co-adsorption of water at titanium sites from the solvation sphere of reactant in solution.[125] For aqueous-phase glucose isomerization in both zero-order and first-order kinetic regimes, the reaction rate constants were three to twelve times lower on hydrophilic Ti-Beta-OH than those of hydrophobic Ti-Beta-F sample (Fig. 7a), reflected by the entropic destabilization and high Gibbs free energies for the transition state of hydride-shift isomerization on zeolite Ti-Beta-OH with the presence of high density of hydrogen-bonded water networks. The consequences of formation of extended hydrogen-bonded networks of water for sugar isomerization catalysis has also been described for Sn-BEA zeolites in water phase.[114,129]

Interestingly, the cooperative effects between hydrophilic pores and water structures exist for alkene epoxidation reactions in the presence of Ti-BEA zeolites.[130,162] Herein, in hydrophilic pores, the specific interactions between water molecules, reactive intermediates and zeolite surface bring the advantage of enhancing catalytic reaction performance. There are 100-fold larger in the rate and selectivity for 1-octene epoxidation on Ti-BEA zeolite containing five silanol groups per unit cell in comparison with the nearly defect-free Ti-BEA catalysts (Fig. 7b).[162] Specifically in this work, the extended hydrogen-bonded networks of water, which are stabilized on the silanol defect sites on hydrophilic Ti-BEA zeolites,

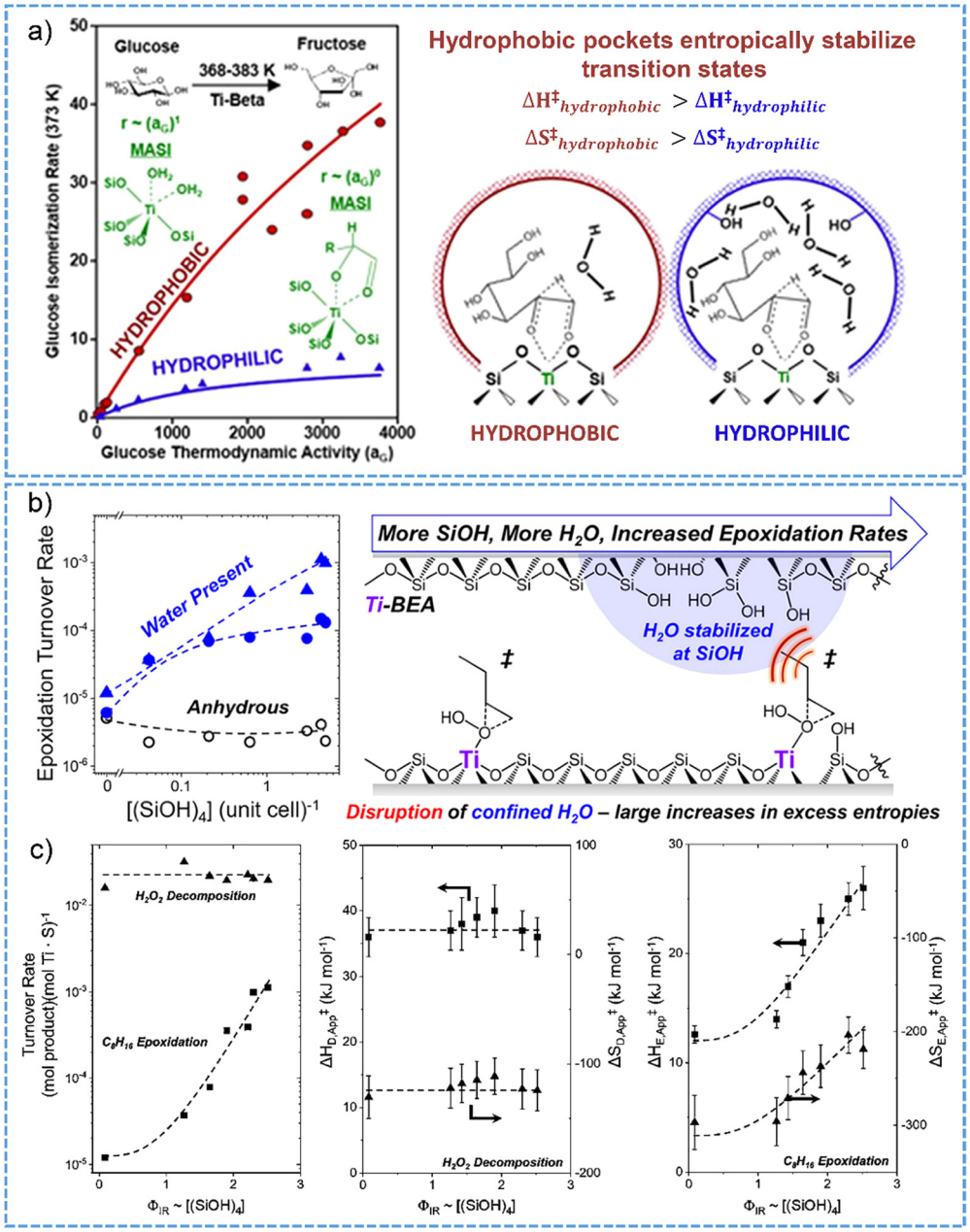


Fig. 7 (a) Glucose isomerization on hydrophobic Ti-BEA shows much higher reaction rates than those obtained on hydrophilic counterparts, owing to the entropic stabilization of transition state by hydrophobic pockets. Reproduced with permission from ref. 125. Copyright 2018, American Chemical Society. (b) Epoxidation of 1-octene with $H_2O_2$ over hydrophilic Ti-BEA zeolites having certain densities of silanol nests exhibits higher turnover rates in comparison with that catalyzed by hydrophobic T-BEA. (c) The turnover rates for 1-octene epoxidation and $H_2O_2$ decomposition at 313 K (left). Apparent activation ethalpies and entropies for $H_2O_2$ decomposition (middle) and 1-octene epoxidation (right) as a function of the factions of $Si(OH)_4$ groups. Reproduced with permission from ref. 162. Copyright 2019, American Chemical Society.

benefit the disruptive interactions between water structures and epoxidation transition states in the pores. The rate of 1-octene epoxidation significantly increased with the increasing amount of silanol nests in the series of Ti-BEA zeolites. The rate of $H_2O_2$ decomposition did not show such dependence as well as the variations of the apparent activation enthalpies and entropies with the silanol nests concentration (Fig. 7c). Notably, a difference by 12 kJ $mol^{-1}$ and 93 J $mol^{-1}$ $K^{-1}$ for the apparent activation enthalpies and entropies were respectively determined between the most hydrophobic and hydrophilic Ti-BEA zeolite catalysts (Fig. 7c). These results imply that the disruptive interactions with water clusters through the reorganization nearby the titanium sites aids in the stabilization of the transition states in zeolite pores, favorably leading to large-increased gains in the excess entropies and the enhanced catalytic epoxidation rates. Knowledge of the specific

 

interactions with the solvent molecules in zeolite micropores can be applicable for other porous materials to enhance catalytic transformations.[130]

**3.2.2. Through impacting the structural properties of zeolite catalysts.** Water structures also manipulate the catalytic reactivity of zeolites through affecting the structures of active site and the nature of zeolite cavities (Scheme 3c and e). Particularly, the extra-framework aluminum species generated from zeolite dealumination (that is the hydrolytic removal of aluminum atoms) during a steaming treatment, as further discussed in detail in Section 4.1, are responsible for enhancements of the catalytic activity. The synergies between Brønsted acid site and extra-framework aluminum are attracting extensive exploitations in the field of zeolite catalysis.[163–166] A typical work by Pham *et al.*[166] reported that the presence of water in zeolite H-MFI could not only hydrolyze framework aluminum to form extra-lattice sites, but also facilitate the migration of extra-framework aluminum to the position closed to the BAS, followed with the formation of synergistic sites for enhancing the *n*-hexane cracking. The authors innovatively applied a micro-pulse technique to introduce water without causing a significant zeolite dealumination and without adjusting zeolitic crystallinity as well as the BAS concentration. Results of catalytic reactivity indicated that zeolites having higher concentration of BAS and extra-framework aluminum species can positively respond to the pulses of water treatment. A strong inhibition on hydrocarbon cracking rate after 50 pulses of water was possibly associated to the adsorption of water on both extra-framework aluminum and synergistic sites by generating ''un-active'' hydrated forms.[166] It should be noted that the origins of Lewis acidic aluminum ions are diverse,[101–106] and the existence of the synergy between the BAS and extra-framework Al ions is still debatable. Some DFT calculation works have been performed to evaluate the changes of Brønsted acidity of bridging hydroxyl groups which are close to the extra-framework Al ions and different or even opposite findings have been reported.[167–170] Despite the positive results for the hydrocarbon cracking reactions,[165,166] much research works are needed to fully understand the origins of the synergy between BAS and extra-framework Al ions on catalytic activities.[171]

Water molecules especially those from liquid hot water can also induce the extensive hydrolysis of zeolite framework structures under catalytic conditions, thereby giving rise to the loss of activity. As reported in the work of Vjunov *et al.*,[172] there were 30–40% decrease of micro- and mesopore volume for zeolite H-BEA (Si/Al = 15–75) after aging in water at 160 °C for 48 h. This change in zeolite structures was associated to the pore blocking *via* framework hydrolysis of Si–O–Si and Si–O–Si–OH groups, and the re-precipitation of silica on crystallite surface. As a result, the accessibility of active BAS sites to cyclohexanol molecules was reduced, leading to a decreased activity for the aqueous-phase alcohol dehydration. The authors stated that the structural and functional stability of zeolites with the presence of intraporous water are important factors determining the activity performance for reactions carried out in liquid hot water.

### 3.3. Impairing catalytic stability of zeolite by intraporous water structures

**Water mitigates coke formation to improve zeolite catalytic stability.** The rapid coke formation is the widely encountered issue at the solid–gas interfaces in a wide variety of catalytic processes such as high-temperature hydrocarbon cracking, methanol-to-hydrocarbon (MTH, including the MTO conversion) and non-oxidative methane dehydroaromatization (MDA) reaction.[173–177] The initially formed ethene and propene in MTO conversion often undergo the reactions of oligomerization and cyclization to secondary products including higher olefins, aromatics and poly-aromatics, which exist as the coke precursors being strongly adsorbed on the acidic sites in zeolite channels and cavities. These coke compounds could block zeolite pores and render the acidic zeolites susceptible to drastic deactivation. There are a body of works highlight the positive impact of water in mitigating coke formation to improve the stability of zeolite catalysis.[133,136,137,178–181] That is, co-fed water or *in situ*-generated water appears to impede the accessibility of the active sites to coke precursors and in turn prevent them from undergoing the polymerization and further growth into coke species in the zeolite pores, thus favoring the catalytic stability of zeolitic materials. Recently, by combining first-principle calculations and *in situ* microspectroscopy, De Wispelaere *et al.*[134] investigated at molecular level the effect of water on the MTO conversion catalyzed by H-SAPO-34 zeolite. Adding water to the feed was found to delay the formation of aromatic hydrocarbon pool species and the subsequent generation of coke species. Water molecules positively enhanced the diffusion of methanol and small olefins into the inner crystals, and it was further concluded to give rise to an efficient use of the active sites with prolonged time on stream (Fig. 8a). The promoting roles of co-feeding of water have also been corroborated for methanol dehydration to dimethyl ether on ferrierite-type zeolite,[182] ethene to aromatics reaction on H-ZSM-5[133] and MDA reaction catalyzed by Mo/H-ZSM-5.[183] As mentioned in Section 3.1 that the structures of water are contingent on the number of water molecules in zeolite cavities and the operation conditions (*e.g.*, temperature, reactant), the role of water in enhancing catalytic stability by the means of regulating coke formation is in need of careful investigations case by case.[133,138]

**Dependence of the catalytic stability of Brønsted acidic zeolite on the concentration of intraporous water clusters.** It is well known that the presence of defect sites can promote the hydrolysis rate of zeolite framework in pure hot liquid water;[184,185] the stability of zeolite is higher the lower the concentration of internal defects. Interestingly, Prodinger *et al.*[186,187] stated that the stability of zeolite H-BEA during the aqueous-phase cyclohexanol dehydration was negatively affected by the concentration of water in the micropores. Unlike the situation in pure water, the concentration of intraporous water in aluminum-rich and aluminum-poor H-BEA varied with the presence of organic molecules dissolved in the aqueous phase. H-BEA materials having a higher Si/Al ratio (*e.g.*, 40, 75) can be loaded with a lower amount of hydronium ions in the

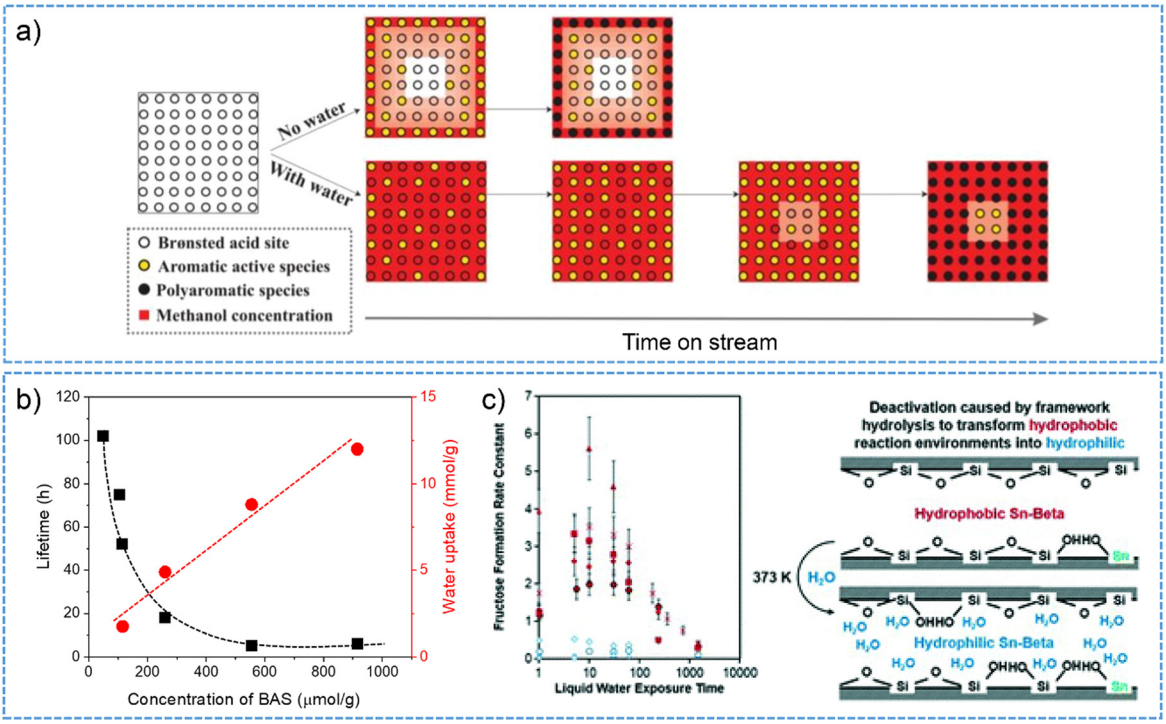


Fig. 8 (a) Schematic illustration for water effect on MTO reaction and the formation of aromatic and polyaromatic species. Reproduced with permission from ref. 134. Copyright 2016, American Chemical Society. (b) Zeolite catalytic lifetime and the uptake of water as a function of the concentration of BAS for different H-BEA zeolites. This plot was drown based on the data points from ref. 187. (c) Structural transformation of hydrophobic to hydrophilic micropores of Sn-BEA causes the catalytic deactivation (as a function of exposure time to liquid water) for aqueous-phase glucose isomerization. Reproduced with permission from ref. 193. Copyright 2019, Royal Society of Chemistry.

pores and consequently exhibited a prolonged lifetime during the catalytic reactions. In contrast, the lifetime of zeolite H-BEA frameworks possessing lower Si/Al ratios (*e.g.*, 12 and 15) displayed negative correlations with respect to the concentration of hydronium ions in zeolite pores.[186] Notably, these results cannot rule out the contribution of defect sites for the varied amount of hydronium ions confined in H-BEA zeolites. The authors further synthesized low-defect H-BEA materials (0.08–0.21 mmol $g^{-1}$ of defect sites) with the presence of fluoride anions, to confirm the critical effect of the concentration of intrazeolite hydronium ions on the catalytic stability of H-BEA for catalyzing alcohol dehydration in aqueous phase (Fig. 8b).[187] These works imply the necessity of systematic studies on zeolite catalytic stability under realistic reaction conditions, where the hydrophilic domains of zeolite pore are filled with water clusters hydrated by the BAS protons and the preserved hydrophobic part act as the adsorption sites for the reacting molecules.

**Changes in the structures of active site and pore polarities induced by water on Lewis acidic zeolites.** The catalytic stability of Lewis acidic zeolites can be associated to some extent with the stability of the local structural property of framework heteroatoms. Interacting with water has been widely reported to change the coordination of tin atoms by forming open form tin sites and hydroxyl groups,[122,188–190] thus synergistically affording the desired catalytic performance for the reaction such as glucose isomerization in aqueous phase.[191] In addition, the positive role of water with the addition of a small amount in methanol solvent (10%, w/w) was identified to improve the catalytic stability of Sn-BEA zeolite by one order of magnitude during the continuous glucose conversion.[192] Water in this system minimizes the changes in the coordination environment and keeps a high degree of the hydration of tin and silica sites on the Sn-BEA zeolite. Furthermore, the transformation from hydrophobic to hydrophilic property for the zeolite Sn-BEA, as a result of the formation of defect sites in the micropores, can be assigned to the decreased reaction rates (that is the poor catalytic stability) for the aqueous-phase glucose isomerization (Fig. 8c).[193] Potential changes of the metal sites and structural functionalities on Lewis acidic zeolite framework under the reaction conditions with the presence of water may, therefore, relate to the different catalytic stabilities for liquid phase reactions, which should be considered with much research attentions.

## 4. Zeolite stability in the presence of water structures

### 4.1. Structural and functional stability of zeolitic materials

**Brønsted acidic zeolites.** This subsection will start by presenting the structural and functional stability of Brønsted acidic zeolites with the presence of water vapor at the solid–gas interfaces. Note that, in addition to internal surface within

 

micropores, the real zeolite catalysts also contain external surface, in particular those having nanometer ranged particle size.[194] The presence of a variety of external surface sites (*e.g.*, Si–OH, Al–OH, Al–$(H_2O)(OH)_n$) and their interactions with water molecules have been reported to result in thermal stability issue and complex the quantification of the amount and acidity of Brønsted and Lewis acid sites.[194–197] Currently, studying the nature and identifying the structure of external surface groups on acidic zeolites have drawn intensive research interests, but the conclusions from these studies are still debatable.[171,198] Due to this fact, the following discussions mainly focus on the structural and functional stability of zeolites within the internal micropores with the presence of adsorbed water molecules.

Exposing to a steam condition at high temperature (above 500 °C) is the method generally adopted on purpose for the preparation of high-performing Brønsted acidic zeolites (*e.g.*, USY and MOR zeolites) and also for the regeneration of spent catalyst materials after the catalytic deactivation, *e.g.*, that in the case of MTO conversion and fluid catalytic cracking.[199,200] Heterogeneous catalytic reactions particularly those applied in petrochemical industry often take place at moderate temperatures ranged from 100 to 500 °C. Relating to the competitive adsorption effect, co-feeding water at the solid–gas interfaces is a decent strategy employed to tackle the issue of coke formation in zeolite pore networks[134–136] and manipulate the catalytic performance of zeolite materials.[133,139] The reversible breaking and formation of T–O–T bonds (*i.e.*, P–O–Al, Si–O–Al) induced by water in the framework of SAPO-34 at moderate-temperature conditions have been revealed by means of $^{17}O$ NMR spectroscopy.[201] The structural dynamic process enables the encapsulation of bulky molecules (*e.g.*, trimethylphosphine (TMP)/pyridine having kinetic diameters larger than the zeolite pore size), which allows the characterization of acidic sites and endows the zeolite with boosted behavior of shape-selective catalysis. On the other hand, it is important for zeolite catalysis to correlate the catalytic properties to the structural changes of zeolite after an exposure in water atmosphere (in gas and liquid phase).[202] Upon exposing the aluminum-containing zeolites to water, framework dealumination through the hydrolysis of Si–O–Al bonds takes place to create dislodged or partially dislodged aluminum species that feature as Lewis acid sites.[203] The extra-framework aluminum species with the forms like $AlO^+$, $Al(OH)_2^+$, $Al(OH)_3$ and $Al_2O_3$ can be created by taking the expense of partially coordinated aluminum atoms after a severe steaming treatment on the zeolite.[166,204] Many of experimental investigations and theoretical calculations have been conducted for better understandings about the stability of zeolite structures when or after contacting with water molecules.[205,206]

Zeolite dealumination may render a decrease in the concentration of functional Si(OH)Al, *i.e.*, the BAS[105,166,204] and in turn an irreversible activity loss of a given catalytic reaction, for example, catalytic cracking catalyzed by Brønsted acid sites.[207] The loss of the BAS is additionally associated with the poisoning effect originating from the extra-framework aluminum species, the latter can be removed by acid-leaching treatment to restore the BAS density to a certain extent.[208] Dealumination events may also deteriorate the acid strength of the site[209] and the crystal porosity or cause pore collapse of zeolite structure.[210–212] Moreover, water even at a small partial pressure in the gas phase (or from the moisture) appears to entangle the identification and quantification of Brønsted and Lewis acidic sites with varied coordination structures on acidic zeolites.[102,103] The conversions of part of tetrahedral aluminum atoms in H-BEA, H-MOR, H-Y zeolite frameworks into aluminum species with octahedral coordination have been intensively observed in the presence of water vapor at room temperature.[212–214] As measured for zeolite H-MOR, the octahedral aluminum atoms formed in a hydration condition are associated to the framework, correlating to the detected Lewis acid sites by FT-IR spectroscopy in a dehydrated environment.[102] Such transformation of framework-associated aluminum enables the switch of Brønsted and Lewis acidity of zeolites and the obtained Lewis acidity can be distinguished with that originated from extra-framework species in zeolites.[103] Recently, through the combination of experimental $^{27}Al$ NMR spectroscopy and biased *ab initio* molecular dynamics (AIMD), it was revealed that the existence of framework-associated octahedral aluminum can be kinetically feasible and thermodynamically stable on H-MOR and H-CHA zeolites only having BAS sites with a close proximity (low Si/Al ratios) (Fig. 9a and b).[215] Moreover, the octahedrally coordinated aluminum species are unstable and they can revert to tetrahedral coordination when the zeolite material is heated to a high temperature (above 383 K),[68] or is ion-exchanged to the sodium or ammonium form.[103,212,214,216,217] Reversible structural changes are a general property for protonic zeolite materials, which largely depend on the procedures involved in sample pretreatment, as summarized based on our recent investigations (Fig. 9c).[103]

As for mechanistic understanding of zeolite structural degradation with the presence of water, computational studies have most commonly considered the single-water hydrolysis mechanism, where exists a stepwise interaction of a single water molecule with the zeolite framework.[218–220] Water coordinating with an aluminum site is crucial for the breakage of Si–O–Al bonds under the steaming conditions. With respect to the single-water hydrolysis mechanism, the first Al–O(H) bond breaking step is initiated with the adsorption of one water molecule on an aluminum atom in anti-position to the BAS, which leads to the formation of aluminum species with a pentahedral or distorted tetrahedral coordination (Scheme 4).[218,220] Subsequent addition of water with up to a number of four enables the successive disconnection of Al–O(H)–Si bonds, thereby giving rise to the generation of dislodged aluminum species (*e.g.*, $Al(OH)_3H_2O$) and silanol nest defects. Dissociative water adsorption and proton transfer are included during the adsorption of the first three water molecules, while the adsorption of the fourth water is non-dissociative without the occurrence of proton transfer. There is a high necessity of performing computational modeling under the realistic conditions (*i.e.*, low-pressure water vapor

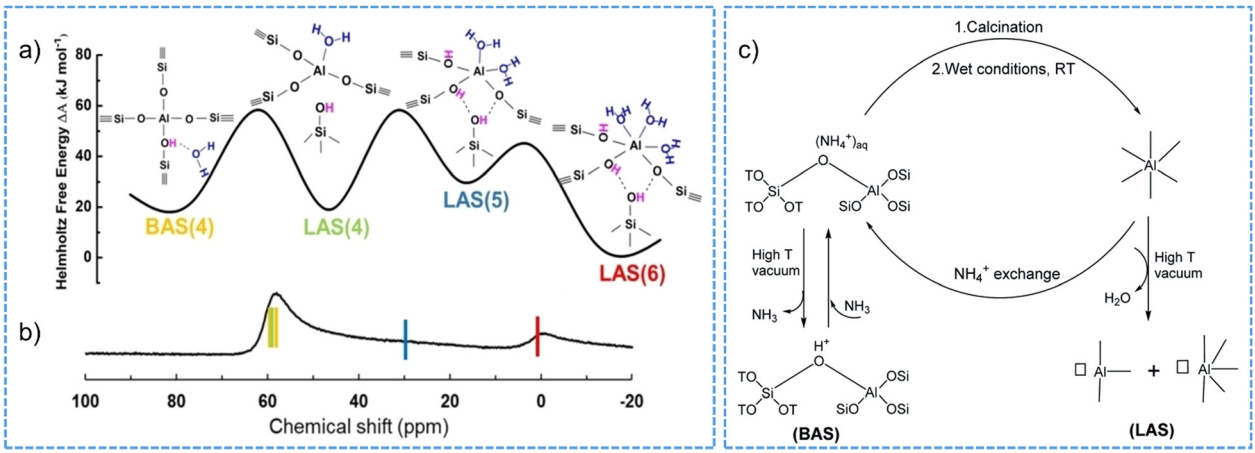


Fig. 9 Structural, thermodynamic (a) and NMR (b) characteristics of tetrahedral and octahedral aluminum in CHA zeolite (Si/Al = 3 and 6 water molecules per cage). BAS: Brønsted acid site. LAS: Lewis acid site. The number in the brackets in (a) represents the number of O in the first coordination shell of Al. Reproduced with permission from ref. 215. Copyright 2023, Wiley-VCH. (c) Schematic illustration of the switch between Brønsted and Lewis acidity of zeolite by the transformation of framework-associated aluminum under different synthetic conditions. Reproduced with permission from ref. 103. Copyright 2021, Royal Society of Chemistry.

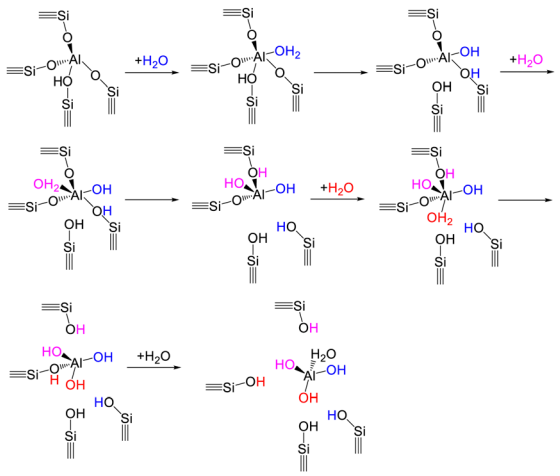

Scheme 4 A proposed single-water hydrolysis mechanism for zeolite dealumination process.[218,220]

or high-pressure condensed water phase), given that the mechanisms of zeolite dealumination differ with water loadings in the zeolite pores.[221] In addition, the regioselectivity of aluminum sites during the process of dealumination are mainly determined by the accessibility of aluminum atoms as well as the reaction conditions in terms of water vapor pressure and temperature.[222] Apart from the dealumination behavior, zeolite desilication under the steaming condition requires the dissociated-adsorption of four water molecules for the formation of extra-framework Si species.[219]

Similar to the behavior in hydrous gas phase, zeolite structures appear to become labile when the pore is subjected to condensed liquid water phase at low-temperature conditions.[223,224] By performing AIMD studies on chabazite (CHA) channels fully loaded with water (15 $H_2O$ per 36 T site supercell), Heard *et al.*[223] investigated the reversible bond-breakage/hydrolysis of Al–O and Si–O bonds in the hydrated zeolite at room temperature. In analogy to that in Scheme 4, the hydrolysis of Al–O bond involves non-dissociative water adsorption on an aluminum site in the anti-position to the BAS, followed by the inversion of $AlO_3{\cdot}H_2O$ tetrahedron (Fig. 10a). The hydrolysis of Si–O bond, which possesses higher free energy barrier than the hydrolysis of Al–O bond, is initiated by the direct interaction of water with silicon through the oxygen atom. Subsequently, a chain of water molecules forms between water within the solvent and the framework oxygen. Proton transfer through water chain to the framework oxygen takes place *via* the Grotthuss mechanism, giving rise to breaking the Si–O bond together with inverting of the $SiO_3OH$ tetrahedron facilitated (Fig. 10a).

The hydrothermal stability of zeolitic materials has been studied by most of the research, since the chemical reactions in aqueous phase are often performed at high temperatures.[225] Upon short immersion of zeolite Y was shown to induce a fast transformation into amorphous material through the hydrolysis of Si–O–Si bonds by the hydroxyl ions in hot water at 150 and 200 °C.[226] Zeolites with dense topologies such as MFI and MOR are more highly resistant toward the degradation in hot water, comparing to the FAU and BEA zeolites with low-density frameworks. Temperature dependence for the degree of zeolite degradation in condensed water phase has been reported for zeolite ZSM-5.[227] Besides, the issue concerning zeolite framework degradation tends to become worse with the increased Si/Al ratios[228] or with the formed hydrophilic silanol groups in the zeolite pores.[226] However, Vjunov *et al.*[184] observed an inverse correlation between the hydrothermal stability and the framework aluminum concentration for zeolite HBEA-12 (Si/Al = 12) and HBEA-75 (Si/Al = 75). Zeolite structural and compositional features such as the distribution of aluminum atoms in lattice, crystal size and the concentration of defects (*i.e.*, silanol nests) were argued to govern the

 

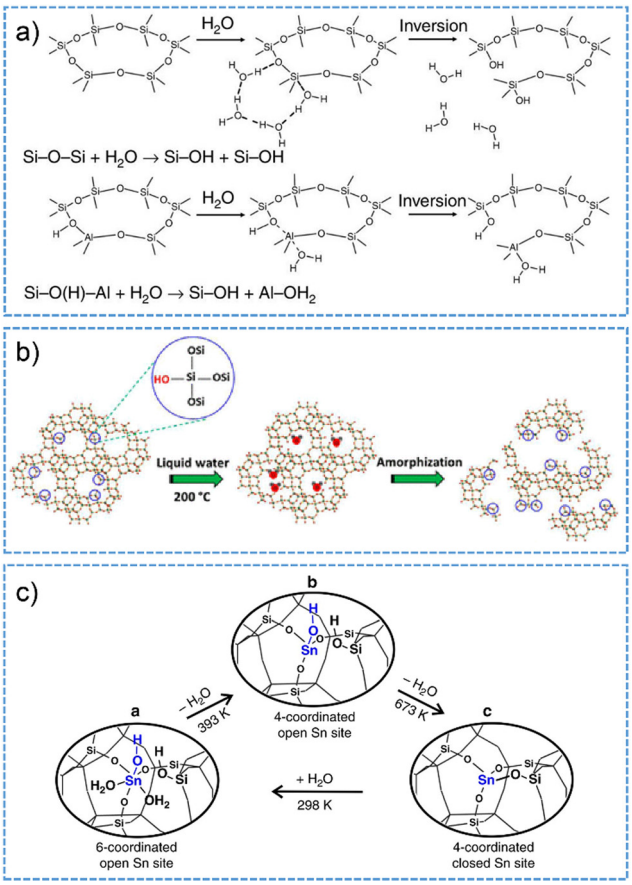


Fig. 10 (a) The mechanism proposed for Si–O and Al–O bond breaking reactions on CHA zeolite in water at room temperature. Reproduced with permission from ref. 223. Copyright 2019, Springer Nature. (b) Schematic illustration for the process of zeolite degradation initiated on silanol defect sites in hot liquid water. Reproduced with permission from ref. 185. Copyright 2015, American Chemical Society. (c) The models for the interconversion between open and closed form Sn sites in Sn-BEA zeolite. a: 6-coordinated open form Sn; b: 4-coordinated open form Sn; c: 4-coodrinated closed form Sn. Reproduced with permission from ref. 190. Copyright 2018, Springer Nature.

HBEA stability in this case. For HBEA degradation process in hot water, it was proposed to be primarily proceeded by the hydrolysis of siloxane T–O–T groups reside in 4-membered rings, leading to the formation of silanol nests and the collapse of pores. Following this is a subsequent Ostwald–ripening process, where amorphous silica layers are formed on the exterior surface. The amorphous domains in the crystal lattice then undergo the internal decomposition and the final breakdown of zeolite pore structures.

The density of silanol defects, rather than the concentration of BAS, Si–O–Si bonds, framework type and extra-framework aluminum, is the dominant characteristic feature responsible for the disintegration of acidic zeolite frameworks in hot liquid water.[185] Silanol defects could facilitate the nucleation of water inside of zeolite pores and thereby promote the hydrolysis of T–O–T groups (Fig. 10b). The loss of structural and functional stability of zeolite can be irreversible in most cases, resulting in a lower degree of zeolite crystallinity and loss of sorption capability. Computational results have shown that the formation of extra-framework silicon is more thermodynamically favorable than the course of zeolite dealumination with the presence of liquid water, which is different to the case when treating zeolite materials under steam. The structure at aluminum sites can therefore be remained to be stable by featuring the tetrahedral coordination without selective removal or substantial redistribution after the treatment in hot liquid water.[172,184,226] Despite the above advances, there are also developments in elucidating the nature of defects on zeolite internal and external surfaces by the means of spectroscopic and computational analysis.[198,229,230] Providing a critical assessment on the research in zeolite defects is beyond the scope of this section and the reader is referred to the recent excellent reviews from the group of Chizallet.[171,198] Since surface defects play important roles in determining the catalytic activities and structural and functional stabilities of zeolitic materials upon contacting with water molecules, comprehensive research efforts in this area are highly desired.

**Lewis acidic zeolites.** Structural transformation of Lewis acidic zeolite when contacting with water usually accounts for the differences in zeolite-catalyzed reaction performance.[110,193,231] As a consequence of the interaction with water, partial hydrolysis of Sn-BEA zeolite was identified to concurrently generate the open form Sn centers (*i.e.*, $(SiO)_3Sn$–OH) which are more catalytically active than the Sn sites with closed form.[188] Water molecules adsorbed on Sn-BEA zeolite have the potential to, in part, transform Lewis acid site into Brønsted acid site, as demonstrated by IR and NMR measurements.[189] Changes in the coordination configuration of Sn with water and the dynamic hydrolysis of Si–O–Sn moieties to Si–OH and Sn–OH sites are responsible for this transformation. The partial hydrolysis of Sn-BEA has been verified to be reversible through gradual dehydration process under high temperatures (Fig. 10c).[190]

The hydrothermal stability of Lewis acidic zeolite in aqueous phase is, in fact, determined by the defect sites introduced either during the material synthesis process or under the catalytic reaction conditions.[193] Typical for zeolite Sn-BEA, the densities of defect sites show a dependency on the framework Sn concentration and they can be hydroxylated to form isolated internal silanol groups when contacting with liquid water molecules.[127] In this way, the extensive hydrolysis of Si–O–Sn bonds is initiated followed by an increase in the uptake of water in zeolite micropores, which in turn promotes the process of framework hydrolysis. For the details on the hydrolysis of heteroatoms-substituted zeolites, the readers are referred to an excellent review by Heard *et al.*[232] Current results convince us that the systematic characterization of the metal sites and their overall structures in the presence of water are essential by considering the establishment of structure–performance correlations for Lewis acidic catalysis.

### 4.2. Synthetic strategies for enhancing zeolite stability

The physicochemical properties of zeolite materials can be tuned generally by modifying the synthetic conditions and

through performing post-synthetic treatments. Note again that, the metal-containing zeolite catalysts are not the main focus of this Review, the approach such as substitution of protons with metal cations (such as $Na^+$, $Cu^+$, $La^{3+}$, *etc.*)[233–235] to strengthen the Al–O bonds and prevent zeolite framework from the attack by water will not be presented in this section. Instead, several typical strategies such as those depicted in Scheme 5 for synthesizing zeolitic catalysts with high structural/catalytic stabilities under steaming conditions or in liquid water phase will be discussed as follows by taking some representative works.

Of the numerous efforts, the introduction of extra-framework phosphorous (P) species has been proved profitable for stabilization of zeolite catalysts with the presence of water, particularly for applications in hydrocarbon cracking.[207,236–239] Wet impregnation of phosphorous precursors (*e.g.*, $H_3PO_4$, $NH_4H_2PO_4$ or $(NH_4)_2HPO_4$) is the commonly applied post-synthetic method for the incorporation of phosphorous species onto zeolite frameworks.[238–240] The dealumination behavior of zeolite upon exposure to a steam condition can be efficiently mitigated by the incorporation of phosphorous species, which thereby aids in obtaining high catalytic performance for the phosphated zeolites.[238] For example, zeolite stabilized by phosphorous element has been applied at much higher temperatures for steam catalytic cracking of naphtha, benefiting in the measured high yield and selectivity to ethane and propene.[237] Phosphorous species are likely protonated by a certain amount of BAS in zeolite to stabilize the aluminum cations in the zeolitic framework (Scheme 5a),[207] while resulting in decreased concentration and strength of the BAS site in most cases.[241–243] Optimization of the content of phosphorous during the synthesis of phosphorous-containing zeolite is desirable to allow for avoiding a significant loss of acidity and catalytic activity/selectivity.[238,239,243] Nevertheless, the interactions between extra-framework phosphorous species and framework aluminum atoms within the zeolite structures remain to be not well understood. The partially dislodged four-coordinated framework aluminum cations have been proposed to facilitate their interactions with the incorporated phosphate species (P–O–Al interactions) in the ZSM-5 zeolite pores.[240,244] Thermal treatment of the zeolite containing P–O–Al interactions at high temperature usually induces the formation of local silico-aluminophosphate interfaces and eventually promotes the hydrothermal stability of phosphated zeolites, as studied by means of multi-spectroscopic technologies including $^{27}Al$ and $^{31}P$ MAS NMR and FT-IR.[240]

Surface overcoating engineering such as the introduction of a hydrophobic barrier layer on the surface of as-synthesized zeolites is expected to be of great interest (Scheme 5b). For example, vapor phase deposition of hydrophobic triphenyl silane could endow BEA zeolite as robust catalyst towards the attack by the steam and thereby achieving high yield of lighter hydrocarbons in steam-assisted catalytic cracking.[245] More recently, Wang *et al.*[246] observed that the silane coatings can potentially protect ZSM-5 zeolite under the hydrothermal conditions at $\leq$300 °C, but these silane coatings provided

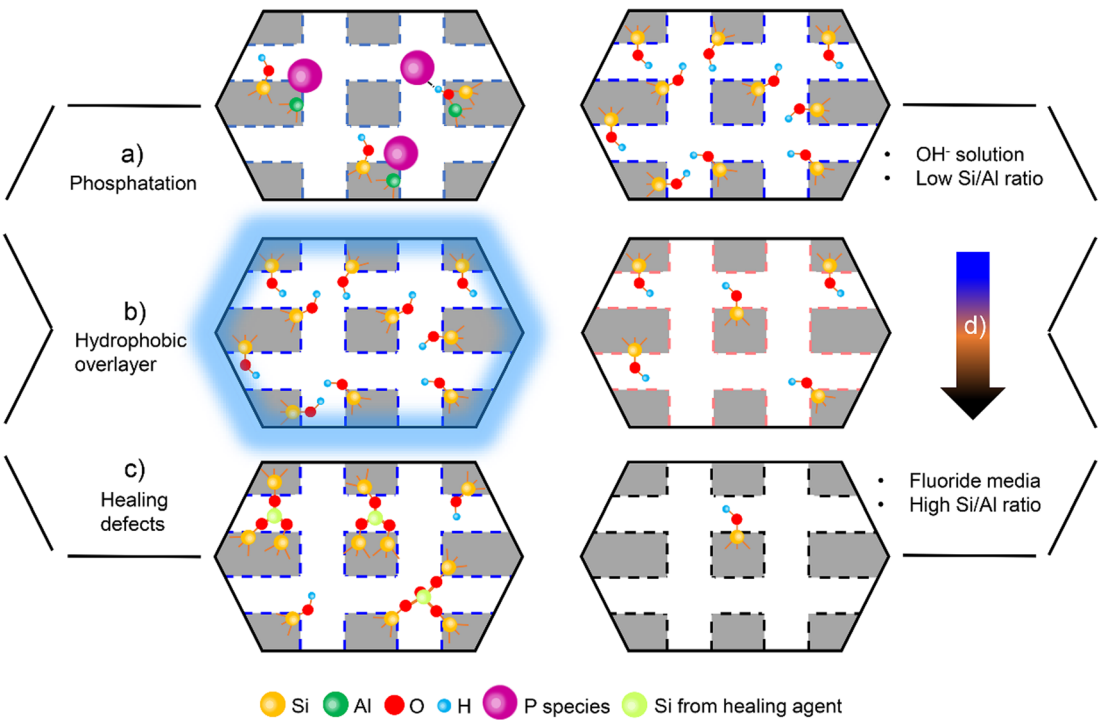


Scheme 5 Overview of strategies aiming at improving zeolite stability when exposed to steam condition or applied in liquid water phase. (a) Phosphorous impregnation of zeolitic materials. (b) Surface overcoating engineering on the external surface of zeolite with hydrophobic matters (*e.g.*, organosilanes, carbon overlayers, *etc.*). (c) Healing of internal silanol defect sites by employing organosilanes. (d) Minimizing of defects on zeolite through changing the synthetic conditions from alkaline solution to fluoride media, or synthesizing the zeolite catalysts with high Si/Al ratios.

 

ineffective protection in the presence of supercritical water (400 °C). Upon the sequence of hydrothermal carbonization with glucose and high-temperature pyrolysis treatment, in this work, the ZSM-5 zeolites were further developed into carbon-coated counterparts to work as the hydrophobic and stable catalysts for dodecane cracking in supercritical water condition.[246] Carbon coating layers with an optimal loading of 10 wt% effectively protected the crystallinity of ZSM-5 zeolite and the BAS sites as well, while exerting the influences on the mass diffusion to a lesser extent in comparison with the samples with higher loadings of carbon overlayers.

Functionalization of zeolite external surface with organosilanes have been potentially applied as an efficient post-synthetic tool to address the stability improvement of Brønsted acidic zeolites under liquid-phase catalytic reaction conditions.[185,187,247,248] The surface properties of the original zeolite can be replaced with that of introduced organosilanes, eventually becoming hydrophobic. For example, Zapata *et al.* improved the hydrophobicity of HY zeolite (Si/Al = 30) by performing the silylation treatment on zeolite surface with a silylating agent, *e.g.*, octadecyltrichlorosilane (OTS).[247] It was emphasized that the acid sites concentration remained unchanged after the selective introduction of hydrophobic OTS layers on the external surface of HY zeolite. Ethyltrichlorosilane (ETS) has also been applied for the silylation of HY-2.6 (Si/Al = 2.6, CBV 600).[185] The stability of functionalized HY zeolites aforementioned were substantially improved by the protection of the internal zeolite pores from contacting with liquid water at 200 °C. In comparison, the parent HY-2.6 zeolite underwent a drastic collapse of the lattice crystal upon a similar treatment in hot water, as indicated by the DRIFT spectra (Fig. 11a). This strategy is flexible, feasible and can be used for the rational design and synthesis of hydrophobic zeolite catalysts by a suitable selection of organosilanes.

In addition to the silylation of the external surface, the direct prevention on Si–O–Si bonds of the hydrolytic attack by water is essential when considering the formation of water with a high rate on the internal space of zeolite crystallites. Prodinger *et al.* reported an effort related to the improvement of zeolite hydrothermal stability by removing the inner structural defects (Scheme 5c).[249] Herein, the internal silanol defects inside of H-BEA were selectively removed by the reaction with trimethylchlorosilane (TMS–Cl). In a flow reactor system, TMS–Cl vapor carried by $N_2$ gas was introduced into H-BEA that were synthesized with certain amounts of Si–OH defect. Upon dosing of TMS–Cl, the Si–OH defect underwent the initial capping by TMS–Cl *via* a condensation reaction. It leads to the decreased

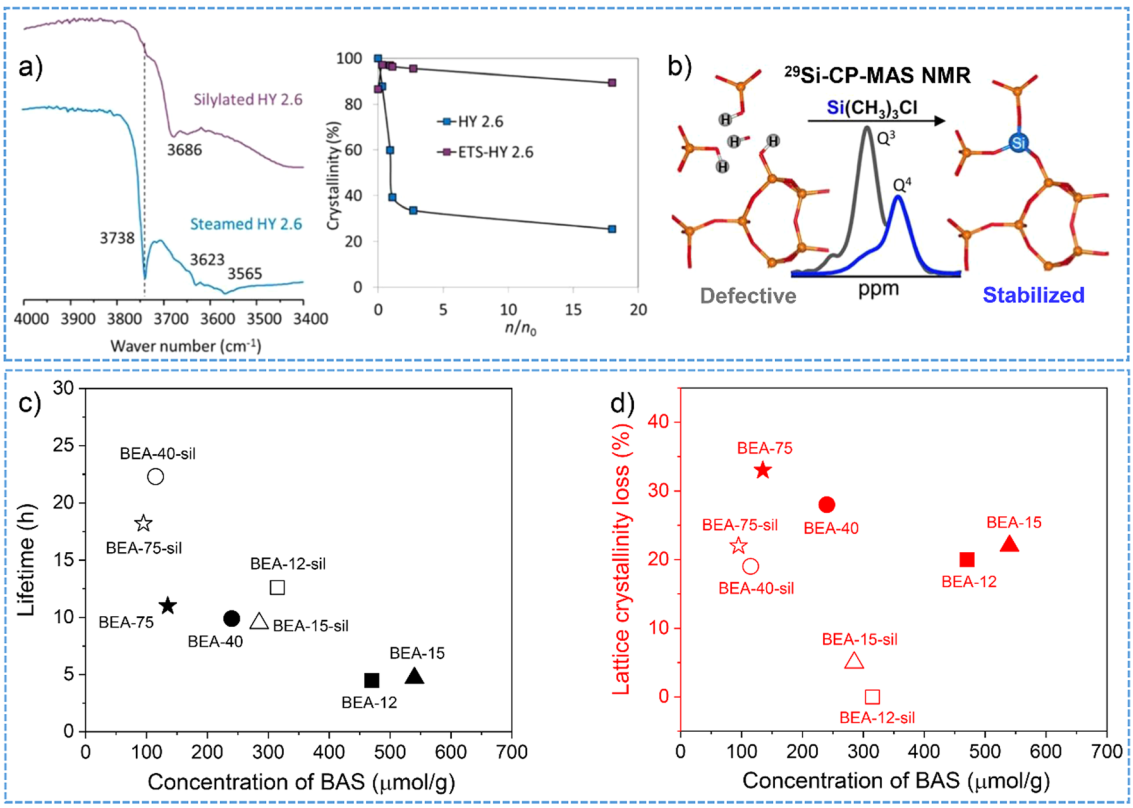


Fig. 11 (a) The collected DRIFT spectra and crystallinity losses for steamed HY 2.6 and the corresponding silylated one upon water attack. Reproduced with permission from ref. 185. Copyright 2015, American Chemical Society. (b) Schematic illustration for the silylation of H-BEA with TMS–Cl for the stabilization of internal SiOH nests. Reproduced with permission from ref. 249. Copyright 2016, American Chemical Society. Comparisons of catalytic lifetime as a function of the BAS concentration during the aqueous-phase cyclohexanol dehydration at 170 °C (c) and lattice crystallinity loss in pure water at 170 °C after 48 h (d). These two plots were drawn based on the data points from ref. 186.

density of $Q^3$ peak at −103 ppm (defect $Si(OH)(OSi)_3$ species) and $Q^2$ peak at −92 ppm ($Si(OH)_2(OSi)_2$ species), as observed from the $^{29}$Si-CP-MAS-NMR spectra (Fig. 11b). This defect healing process involves the formation of Si–O–Si bonds and the release of methane consequently, as suggested by the identification of primary, secondary and tertiary silylation products with different chemical shifts. Enhanced stability was indicated by the combined characterizations on lattice crystallinity, microporosity and mesoporosity of the silylated BEA zeolites after the treatment in liquid water at 160 °C for 48 h.[249] In the following work, silylation-treated BEA with TMS–Cl were reported to show much longer lifetime in aqueous-phase catalytic reactions and less lattice crystallinity loss in pure hot water than their parent defected counterparts (Fig. 11c and d). It was concluded to be the consequences of decreasing the defect densities and reducing the access to water molecules after the treatment of defected BEA zeolite with TMS–Cl.[186] This protocol is expected to be applicable for the defect healing of other kinds of zeolite materials to achieve the improvements of hydrothermal stability.

Apart from above approaches, minimizing the concentration of defects and decreasing the amount of hydronium ions in the pores by direct synthesis strategy aid in the improvement of thermal stability of zeolite materials in hot liquid water (Scheme 5d). The utilization of fluoride anions in the synthesis of aluminosilicate and hydrophobic Lewis acidic zeolites is effective in mitigating the formation of defect sites in zeolite pore networks.[78,113,231,250] Typically selected as an example, H-BEA zeolites with the Si/Al ratios range from 15 to 230 were synthesized with the presence of fluoride anions and the corresponding defect concentrations were characterized to gradually decrease from 210 to 45 μmol $g^{-1}$, in contrast to that (380 μmol $g^{-1}$) of H-BEA-15 sample prepared in an alkaline medium.[187] These low-defective H-BEA zeolites exhibited a high resistance toward the disintegration in aqueous phase for Brønsted acid-catalyzed reactions. Synthesizing zeolitic materials with hydrophobic properties by increasing the Si/Al ratios is another effective way to improve their hydrothermal endurance (Scheme 5d). Nevertheless, these strategies cannot be efficiently reliable to attain the defect-free zeolites and further enable a satisfactory structural stability in hot liquid water. On the other hand, aluminum-free materials such as Sn-BEA and Sn-MFI have been widely synthesized as the stable Lewis acidic zeolites for heterogeneously catalyzing the chemical reactions in water.[231] In most cases, researchers attribute their unique catalytic performance to the hydrophobic properties of zeolite surface and the suitable Lewis acidity that are originated from the substituted atoms in the zeolitic frameworks.[110,115,125,162]

## 5. Summary and outlook

Water as a reactant, by product and solvent could make a difference for heterogeneously catalyzed reactions. Previous studies of zeolite catalysis with the presence of water have highlighted the importance of understanding water structures on acidic zeolites. The interaction of a water molecule with the Brønsted acid site (BAS) on zeolite is initiated with the formation of hydrogen-bonded monomeric complex inside the pores. Increasing the dosages of water in zeolite channels results in the generation of larger-sized water clusters, in which water molecules are protonated by the BAS protons transferred from the framework oxygen. Experimental technologies such as NMR, gas-phase calorimetry, adsorption uptake along with theoretical calculations have verified that the hydrated hydronium ions are composed of eight or ten $H_2O$ molecules per the BAS site. Less numbers of water molecules are identified to be stabilized on each of tetravalent framework heteroatom, *e.g.*, tin, titanium for the case of Lewis acidic zeolites. On Brønsted and Lewis acidic zeolite, framework defects (*i.e.*, silanol nests) those are created either during hydrothermal synthesis or under post-synthetic/reaction conditions, endow the zeolitic micropores with hydrophilic property and further promotes water adsorption uptake. In addition to the water clusters strongly interacting with zeolite framework, extended hydrogen-bonded water networks can be subsequently formed with the additional water molecules in the pores. Confinement effect in zeolite leads to the enhanced proton mobility for the intraporous water clusters that are chemically different from those in the gas phase. The character of framework heteroatoms, zeolite topologies and the concentration of framework defects mainly determine the shape and H-bonding configuration of water structures in acidic zeolite pores.

Water may play positive or dubious roles in the process of heterogeneous catalysis, which is reliant on different catalytic processes and reaction conditions. Water adsorption on the surface or pores of zeolite brings in competitive adsorption phenomena, from which the adsorption behavior of reactants, intermediates and products are substantially tailored. The consequences can be classified to the following aspects including: (a) the loss of accessibility of active site to the reacting molecules; (b) the tailored nature of active sites after the solvation of acidic BAS protons by water; (c) the modifications on the reactant adsorption kinetics that are responsible for activation barriers; (d) the inhibition of coke formation particularly at the solid–gas interfaces (hence maintaining a good catalytic stability). Water clusters likely participate in the formation of water cluster-reactant complexes/clusters with, *e.g.*, low-carbon chain alcohol molecules, which requires extensive disruption of hydrogen bonds and results in inhibitive role of water in gas-phase alcohol dehydration. In addition, the presence of water structures in the nano-environment of zeolite confined spaces could induce thermodynamic non-idealities to the catalytic reactions. To take as the example, manipulating the highly ionic environment in H-ZSM-5 micropores benefited the determined negative value of excess Gibbs free energies for the transition state, which leads to decreased activation energies and in turn enhanced catalytic turnover rates. Analogously, extended hydrogen-bonded water networks fabricated when exposing in water solvent make differences for the enthalpic or entropic stabilization/destabilization of adsorption and

 

transition states on the Lewis acidic zeolites with unique hydrophilic/hydrophobic characters. Interacting zeolite with water vapor or condensed water phase at high temperature often renders the hydrolysis of framework heteroatoms irreversible, which remains as an important subject of zeolite research. Recent progresses on computational modeling have indicated that not only a single water but also intraporous water clusters in the zeolite channels are responsible for the dynamic evolution of Brønsted acidic zeolite structures. The mechanisms with respect to the dealumination and desilication processes in the presence of water differ significantly from each other. Zeolite degradation when contacting with hot liquid water is typically reflected by the transformation of hydrophobic property into hydrophilic one, the loss of lattice crystallinity as well as the structural porosity. In addition to the dependences of temperature and framework density, the concentration of defect sites in zeolite pores acts as the critical factor determining the degree of structural degradation. The correlations of zeolite lifetime as a function of the concentration of properly confined hydronium ions or the changes in the hydrophobicity of molecularly-sized pores are desirable for acidic chemistry in condensed aqueous phase. Rational design of structurally/catalytically stable zeolitic materials will open up a broader perspective for innovative development of new heterogeneous processes in the aqueous phase. Achieving this has potentially involved the synthesizing low-defect or defect-free zeolites and the hydrophobic-functionalizing zeolite surface through post-synthetic approaches such as the impregnation with phosphorous element and catalyst overcoating engineering with hydrophobic organic (*e.g.*, organosilanes) or inorganic (*e.g.*, carbon) overlayers.

Catalyst structures determine the catalytic performance and the reaction mechanisms. Conventional spectroscopic techniques such as NMR and FTIR spectroscopy have been employed to analyze the initial and final structure of zeolite materials. The obtained catalytic data can be the consequence of many factors originated from the evolution of active sites, *i.e.*, Brønsted and Lewis acidic sites in zeolites during catalytic reactions (even without the presence of water molecules), thus making it challenging to establish precisely the structure–performance relationships.[101,171] Performing *in situ* and *operando* characterizations to gain the knowledge on the number, location and structure of different type of active sites, particularly the extra-framework aluminum species in the zeolite pores could pave the way for unveiling the underlying reaction mechanisms and designing of stable zeolite materials. First-principles calculations will continue to be the effective approach to study the process dynamics taking place on catalyst surface and help to solve the unanswered open questions about the identification of diverse active sites on both external and internal surface and their synergistic effects (*e.g.*, the synergy of BAS-LAS pairs) on zeolite acid-catalyzed applications.

Future research directions for the susceptibility of zeolites when applied/exposed in catalytic reaction conditions have been provided above, great efforts are also needed to address the water–zeolite interactions and the corresponding roles in zeolite catalysis. Owing to the several advantages of conducting zeolite-catalyzed reactions with water co-feeding or in condensed water phase, a great number of heterogeneous catalytic reactions such as those catalyzed by metal-supported catalysts are being explored increasingly.[5,251–254] Diverse important catalytic transformations can be expanded to be performed with the presence of gaseous water or in aqueous phase. In this context, the green-valorization of biosourced compounds and manufacturing of high-value fine chemicals will be expectedly favored. It has been reported for zeolite materials that any exposure to gaseous and liquid water during the zeolite lifetime, *i.e.*, zeolite hydrothermal synthesis, zeolite catalysis, regeneration, *etc.* can significantly modify the structural properties of active sites and finally manipulate their catalytic performance.[18,126,162,186,187,202,223] In addition, the local reaction environment involving water molecules in zeolite pores is varied with the nature of active sites and reacting molecules, zeolite topologies, and reaction conditions, which necessitates the systematical understanding about the promotional roles of water on the catalytic reactions of interest. Catalyst characterization technologies are often conducted in vacuum or in inert gas environments, which cannot provide the direct evidences for the catalytic mechanism of the reactions performed under realistic conditions with the presence of water at high temperatures. Better mechanistic insights from experimental studies as well as computational investigations on the structures of solid–water and solid–gas interfaces are highly desirable. Comparing solid–gas interface characterization, the development of *in situ* and time-resolved technologies including XAS (both near edge (XANES) and fine structure (EXAFS)), X-ray emission spectroscopy (XES), scanning probe microscopies for the catalytic processes at solid–liquid interfaces are challenging or are still under development.[255] A combination of calorimetry, thermogravimetric analysis, attenuated total reflection (ATR)-FTIR and solid state NMR possess the potential to facilitate the quantitative comparison of substrate behaviors and to monitor the reaction progress at the solid–liquid interfaces. Kinetic and thermodynamic insights in addition to the catalyst structural information are also essential for understanding the effects of water structures on determining the activation barriers of each elementary steps and controlling over the reaction rate of a catalytic reaction. Decoupling of thermodynamic terms such as solvation, adsorption and sorbate interactions around the active site has been emphasized for the structure–activity relationships that can be established.[145,146,256] There are examples observing differences in the size of hydrated hydronium ions confined in different zeolite topologies and the obvious destabilization effects on sorbed substrates.[95,97] There is a pressing need to perform more detailed investigations on the structure of hydronium ion clusters in porous materials and to unveil how the generated nano-environment causes the non-idealities to a catalytic system. Apart from the sorption and reaction steps in the catalytic cycle, diffusion or mass transport of reactive molecules and products may be responsible for the observed catalytic performance in terms of activity, product

selectivity and catalytic stability.[257–259] At the moment, very few works have addressed the role of water molecules in influencing the diffusivity of reactants, intermediates and products in zeolite pores.[153,154] More insights into the effects of water structures in the diffusion behaviors within zeolite pores remain to be provided in the future research.[171,260] Moreover, by increasing the model complexity under the realistic catalytic conditions and combining different theoretical methods including density functional theory calculations and molecular dynamics simulations,[260] molecular level understandings for the catalytic reactions catalyzed by acidic zeolites with the presence of water can be achieved. Fundamental understanding of water structures and the roles of water molecules in heterogeneous catalysis can benefit the *de novo* design of highly active and stable zeolite and other solid materials for potential catalytic transformations performed in water vapor or in bulk aqueous phase.

## Author contributions

Q. Liu: conceptualization, writing – original draft, writing – review & editing. J. A. van Bokhoven: conceptualization, supervision, writing – review & editing.

## Conflicts of interest

There are no conflicts to declare.

## Acknowledgements

There is no funding or financial support for the present work to declare.

## References

1 J. R. Di Iorio, B. A. Johnson and Y. Román-Leshkov, *J. Am. Chem. Soc.*, 2020, **142**, 19379–19392.
2 J. S. Bates and R. Gounder, *Chem. Sci.*, 2021, **12**, 4699–4708.
3 D. S. Potts, D. T. Bregante, J. S. Adams, C. Torres and D. W. Flaherty, *Chem. Soc. Rev.*, 2021, **50**, 12308–12337.
4 G. Li, B. Wang and D. E. Resasco, *ACS Catal.*, 2020, **10**, 1294–1309.
5 L. Lin, Y. Ge, H. Zhang, M. Wang, D. Xiao and D. Ma, *JACS Au*, 2021, **1**, 1834–1848.
6 E. Barry, R. Burns, W. Chen, G. X. De Hoe, J. M. M. De Oca, J. J. de Pablo, J. Dombrowski, J. W. Elam, A. M. Felts, G. Galli, J. Hack, Q. He, X. He, E. Hoenig, A. Iscen, B. Kash, H. H. Kung, N. H. C. Lewis, C. Liu, X. Ma, A. Mane, A. B. F. Martinson, K. L. Mulfort, J. Murphy, K. Mølhave, P. Nealey, Y. Qiao, V. Rozyyev, G. C. Schatz, S. J. Sibener, D. Talapin, D. M. Tiede, M. V. Tirrell, A. Tokmakoff, G. A. Voth, Z. Wang, Z. Ye, M. Yesibolati, N. J. Zaluzec and S. B. Darling, *Chem. Rev.*, 2021, **121**, 9450–9501.
7 P. Cheung, A. Bhan, G. J. Sunley and E. Iglesia, *Angew. Chem., Int. Ed.*, 2006, **45**, 1617–1620.
8 J. F. DeWilde, H. Chiang, D. A. Hickman, C. R. Ho and A. Bhan, *ACS Catal.*, 2013, **3**, 798–807.
9 C. J. Baranowski, T. Fovanna, M. Roger, M. Signorile, J. McCaig, A. M. Bahmanpour, D. Ferri and O. Kröcher, *ACS Catal.*, 2020, **10**, 8106–8119.
10 H. Li, D. Guo, N. Ulumuddin, N. R. Jaegers, J. Sun, B. Peng, J.-S. McEwen, J. Hu and Y. Wang, *JACS Au*, 2021, **1**, 1471–1487.
11 Y. Liu, E. Baráth, H. Shi, J. Hu, D. M. Camaioni and J. A. Lercher, *Nat. Catal.*, 2018, **1**, 141–147.
12 S. K. Desai, V. Pallassana and M. Neurock, *J. Phys. Chem. B*, 2001, **105**, 9171–9182.
13 Y. Yoon, R. Rousseau, R. S. Weber, D. Mei and J. A. Lercher, *J. Am. Chem. Soc.*, 2014, **136**, 10287–10298.
14 Y. Wang, J. Yao, H. Li, D. Su and M. Antonietti, *J. Am. Chem. Soc.*, 2011, **133**, 2362–2365.
15 Z. Zhao, R. Bababrik, W. Xue, Y. Li, N. M. Briggs, D.-T. Nguyen, U. Nguyen, S. P. Crossley, S. Wang, B. Wang and D. E. Resasco, *Nat. Catal.*, 2019, **2**, 431–436.
16 C. Sievers, Y. Noda, L. Qi, E. M. Albuquerque, R. M. Rioux and S. L. Scott, *ACS Catal.*, 2016, **6**, 8286–8307.
17 A. Martínez-Hernández, G. A. Fuentes and S. A. Gómez, *Appl. Catal., B*, 2015, 465–474.
18 K. Stanciakova and B. M. Weckhuysen, *Trends Chem.*, 2021, **3**, 456–468.
19 M. E. Davis, *Nature*, 2002, **417**, 813–821.
20 Y. Li and J. Yu, *Chem. Rev.*, 2014, **114**, 7268–7316.
21 R. M. Barrer, *J. Chem. Soc.*, 1948, **2158**, 2163.
22 P. Tian, Y. Wei, M. Ye and Z. Liu, *ACS Catal.*, 2015, **5**, 1922–1938.
23 M. Moliner, C. Martínez and A. Corma, *Chem. Mater.*, 2014, **26**, 246–258.
24 E. T. C. Vogt and B. M. Weckhuysen, *Chem. Soc. Rev.*, 2015, **44**, 7342–7370.
25 D. T. Bregante, N. E. Thornburg, J. M. Notestein and D. W. Flaherty, *ACS Catal.*, 2018, **8**, 2995–3010.
26 P. Ferri, C. Li, R. Millán, J. Martínez-Triguero, M. Moliner, M. Boronat and A. Corma, *Angew. Chem., Int. Ed.*, 2020, **59**, 19708–19715.
27 Y. Chai, W. Dai, G. Wu, N. Guan and L. Li, *Acc. Chem. Res.*, 2021, **54**, 2894–2904.
28 H. Kobayashi, H. Yokoyama, B. Feng and A. Fukuoka, *Green Chem.*, 2015, **17**, 2732–2735.
29 S. S. Poly, S. M. A. Hakim Siddiki, A. S. Touchy, S. Yasumura, T. Toyao, Z. Maeno and K.-I. Shimizu, *J. Catal.*, 2018, **368**, 145–154.
30 T. Yumura, Y. Hirose, T. Wakasugi, Y. Kuroda and H. Kobayashi, *ACS Catal.*, 2016, **6**, 2487–2495.
31 D. Palagin, V. L. Sushkevich and J. A. van Bokhoven, *ACS Catal.*, 2019, **9**, 10365–10374.
32 V. L. Sushkevich and J. A. van Bokhoven, *Catal. Sci. Technol.*, 2020, **10**, 382–390.
33 Y. Liu, W. Xue, S. Seo, X. Tan, D. Mei, C.-J. Liu, I.-S. Nam and S. B. Hong, *Appl. Catal., B*, 2021, **294**, 120244.
34 H. Lee, R. J. G. Nuguid, S. W. Jeon, H. S. Kim, K. H. Hwang, O. Kröcher, D. Ferri and D. H. Kim, *Chem. Commun.*, 2022, **58**, 6610–6613.

 

35 J. Imbao, J. A. van Bokhoven, A. Clark and M. Nachtegaal, *Nat. Commun.*, 2020, **11**, 1118.
36 J. Imbao, J. A. van Bokhoven and M. Nachtegaal, *ACS Catal.*, 2021, **11**, 8684–8691.
37 E. B. Clatworthy, S. V. Konnov, F. Dubray, N. Nesterenko, J.-P. Gilson and S. Mintova, *Angew. Chem., Int. Ed.*, 2020, **59**, 19414–19432.
38 Z.-P. Hu, J. Han, Y. Wei and Z. Liu, *ACS Catal.*, 2022, **12**, 5060–5076.
39 D. E. Resasco, S. P. Crossley, B. Wang and J. L. White, *Catal. Rev.*, 2021, **63**, 302–362.
40 W. O. Haag, R. M. Lago and P. B. Weisz, *Nature*, 1984, **309**, 589–591.
41 S. Schallmoser, T. Ikuno, M. F. Wagenhofer, R. Kolvenbach, G. L. Haller, M. Sanchez-Sanchez and J. A. Lercher, *J. Catal.*, 2014, **316**, 93–102.
42 D. Liu, A. Bhan, M. Tsapatsis and S. A. Hashimi, *ACS Catal.*, 2011, **1**, 7–17.
43 A. J. Jones and E. Iglesia, *Angew. Chem., Int. Ed.*, 2014, **53**, 12177–12181.
44 T. N. Pham, T. Sooknoi, S. P. Crossley and D. E. Resasco, *ACS Catal.*, 2013, **3**, 2456–2473.
45 A. Gumidyala, T. Sooknoi and S. Crossley, *J. Catal.*, 2016, **340**, 76–84.
46 M. Milina, S. Mitchell and J. Pérez-Ramírez, *Catal. Today*, 2014, **235**, 176–183.
47 M. Yang, D. Fan, Y. Wei, P. Tian and Z. Liu, *Adv. Mater.*, 2019, **31**, 1902181.
48 I. Yarulina, A. D. Chowdhury, F. Meirer, B. M. Weckhuysen and J. Gascon, *Nat. Catal.*, 2018, **1**, 398–411.
49 A. Zecchina, F. Geobaldo, G. Spoto, S. Bordiga, G. Ricchiardi, R. Buzzoni and G. Petrini, *J. Phys. Chem.*, 1996, **100**, 16584–16599.
50 A. Ison and R. J. Gorte, *J. Catal.*, 1984, **89**, 150–158.
51 L. Smith, A. K. Cheetham, R. E. Morris, L. Marchese, J. M. Thomas, P. A. Wright and J. Chen, *Science*, 1996, **271**, 799–802.
52 V. Semmer-Herlédan, L. Heeribout, P. Batamack, C. Dorémieux-Morin, J. Fraissard, A. Gola and E. Benazzi, *Micro. Meso. Mater.*, 2000, **34**, 157–169.
53 S. Bordiga, L. Regli, C. Lamberti and A. Zecchina, *J. Phys. Chem. B*, 2005, **109**, 7724–7732.
54 V. Bolis and C. Busco, *J. Phys. Chem. B*, 2006, **110**, 14849–14859.
55 L. Heeribout, V. Semmer, P. Batamack, C. Dorémieux-Morin, J. Fraissard and G. Antos, *J. Chem. Soc., Faraday Trans., 1*, 1995, **91**, 3933–3940.
56 L. Heeribout, C. Dorémieux-Morin, J.-P. Nogier, R. Vincent and J. Fraissard, *Micro. Meso. Mater.*, 1998, **24**, 101–112.
57 A. Jentys, G. Warecka and J. A. Lercher, *J. Mol. Catal.*, 1989, **51**, 309–327.
58 A. Jentys, G. Warecka, M. Derewinski and J. A. Lercher, *J. Phys. Chem.*, 1989, **93**, 4837–4843.
59 A. G. Pelmenschikov, J. H. M. C. van Wolput, J. Jaenchen and R. A. van Santen, *J. Phys. Chem.*, 1995, **99**, 3612–3617.
60 A. G. Pelmenschikov and R. A. van Santen, *J. Phys. Chem.*, 1993, **97**, 10678–10680.
61 M. J. Rice, A. K. Chakraborty and A. T. Bell, *J. Phys. Chem. A*, 1998, **102**, 7498–7504.
62 L. Marchese, J. Chen, P. A. Wright and J. M. Thomas, *J. Phys. Chem.*, 1993, **97**, 8109–8112.
63 M. Krossner and J. Sauer, *J. Phys. Chem.*, 1996, **100**, 6199–6211.
64 S. A. Zygmunt, *J. Phys. Chem. B*, 2001, **105**, 3034–3038.
65 F. Wakabayashi, *J. Phys. Chem.*, 1996, **100**, 1442–1444.
66 M. V. Vener, X. Rozanska and J. Sauer, *Phys. Chem. Chem. Phys.*, 2009, **11**, 1702–1712.
67 P. Sazama, Z. Tvarůžková, H. Jirglová and Z. Sobalík, *Stud. Surf. Sci. Catal.*, 2008, **174**, 821–824.
68 A. Vjunov, M. Wang, N. Govind, T. Huthwelker, H. Shi, D. Mei, J. L. Fulton and J. A. Lercher, *Chem. Mater.*, 2017, **29**, 9030–9042.
69 M. Jiménez-Ruiz, D. S. Gahle, T. Lemishko, S. Valencia, G. Sastre and F. Rey, *J. Phys. Chem. C*, 2020, **124**, 5436–5443.
70 A. Zecchina, R. Buzzoni, S. Bordiga, F. Geobaldo, D. Scarano, G. Ricchiardi and G. Spoto, *Stud. Surf. Sci. Catal.*, 1995, **97**, 213–222.
71 J. N. Kondo, M. Iizuka and K. Domen, *Langmuir*, 1997, **13**, 747–750.
72 D. H. Olson, S. A. Zygmunt, M. K. Erhardt, L. A. Curtiss and L. E. Iton, *Zeolites*, 1997, **18**, 347–349.
73 Y. Jeanvoine, J. G. Ángyán, G. Kresse and J. Hafner, *J. Phys. Chem. B*, 1998, **102**, 7307–7310.
74 P. W. Kletnieks, J. O. Ehresmann, J. B. Nicholas and J. F. Haw, *ChemPhysChem*, 2006, **7**, 114–116.
75 K. L. Joshi, G. Psofogiannakis, A. C. T. van Duin and S. Raman, *Phys. Chem. Chem. Phys.*, 2014, **16**, 18433–18441.
76 D. H. Olson, W. O. Haag and R. M. Lago, *J. Catal.*, 1980, **61**, 390–396.
77 D. H. Olson, W. O. Haag and W. S. Borghard, *Micro. Meso. Mater.*, 2000, **35–36**, 435–446.
78 K. Zhang, R. P. Lively, J. D. Noel, M. E. Dose, B. A. McCool, R. R. Chance and W. J. Koros, *Langmuir*, 2012, **28**, 8664–8673.
79 S. Jungsuttiwong, J. Limtrakul and T. N. Truong, *J. Phys. Chem. B*, 2005, **109**, 13342–13351.
80 D. Mei and J. A. Lercher, *J. Phys. Chem. C*, 2019, **123**, 25255–25266.
81 D. Mei and J. A. Lercher, *AIChE J.*, 2017, **63**, 172–184.
82 P. Bai, M. Neurock and J. I. Siepmann, *J. Phys. Chem. C*, 2021, **125**, 6090–6098.
83 V. Termath, F. Haase, J. Sauer, J. Hutter and M. Parrinello, *J. Am. Chem. Soc.*, 1998, **120**, 8512–8516.
84 P. Liu and D. Mei, *J. Phys. Chem. C*, 2020, **124**, 22568–22576.
85 J. H. Hack, X. Ma, Y. Chen, J. P. Dombrowski, N. H. C. Lewis, C. Li, H. H. Kung, G. A. Voth and A. Tokmakoff, *J. Phys. Chem. C*, 2023, **127**, 16175–16186.
86 R. C. Shiery and D. C. Cantu, *J. Phys. Chem. C*, 2023, **127**, 4218–4224.

87 C. J. Heard, L. Grajciar and P. Nachtigall, *Chem. Sci.*, 2019, **10**, 5705–5711.
88 M. Wang, N. R. Jaegers, M.-S. Lee, C. Wan, J. Z. Hu, H. Shi, D. Mei, S. D. Burton, D. M. Camaioni, O. Y. Gutiérrez, V.-A. Glezakou, R. Rousseau, Y. Wang and J. A. Lercher, *J. Am. Chem. Soc.*, 2019, **141**, 3444–3455.
89 T. Humplik, R. Raj, S. C. Maroo, T. Laoui and E. N. Wang, *Langmuir*, 2014, **30**, 6446–6453.
90 Z. Li, D. Dittmann, C. Rieg, M. Benz and M. Dyballa, *Catal. Sci. Technol.*, 2022, **12**, 5189–5202.
91 N. Y. Chen, *J. Phys. Chem.*, 1976, **80**, 60–64.
92 T. Sano, N. Yamashita, Y. Iwami, K. Takeda and Y. Kawakami, *Zeolites*, 1996, **16**, 258–264.
93 T. Sano, T. Kasuno, K. Takeda, S. Arazaki and Y. Kawakami, *Stud. Surf. Sci. Catal.*, 1997, **105**, 1771–1778.
94 K. Chen, J. Kelsey, J. L. White, L. Zhang and D. Resasco, *ACS Catal.*, 2015, **5**, 7480–7487.
95 S. Eckstein, P. H. Hintermeier, R. Zhao, E. Baráth, H. Shi, Y. Liu and J. A. Lercher, *Angew. Chem., Int. Ed.*, 2019, **58**, 3450–3455.
96 J. S. Bates, B. C. Bukowski, J. Greeley and R. Gounder, *Chem. Sci.*, 2020, **11**, 7102–7122.
97 S. Kim, N. R. Jaegers, W. Hu, J. Z. Hu, F. Chen, Q. Liu, D. M. Camaioni, M. A. Derewinski, O. Y. Gutiérrez, Y. Liu and J. A. Lercher, *J. Phys. Chem. C*, 2023, **127**, 23390–23399.
98 E. Grifoni, G. M. Piccini, J. A. Lercher, V.-A. Glezakou, R. Rousseau and M. Parrinello, *Nat. Commun.*, 2021, **12**, 2630.
99 N. Pfriem, P. H. Hintermeier, S. Eckstein, S. Kim, Q. Liu, H. Shi, L. Milakovic, Y. Liu, G. L. Haller, E. Baráth, Y. Liu and J. A. Lercher, *Science*, 2021, **372**, 952–957.
100 J. H. Hack, J. P. Dombrowski, X. Ma, Y. Chen, N. H. C. Lewis, W. B. Carpenter, C. Li, G. A. Voth, H. H. Kung and A. Tokmakoff, *J. Am. Chem. Soc.*, 2021, **143**, 10203–10213.
101 M. Ravi, V. L. Sushkevich and J. A. van Bokhoven, *Nat. Mater.*, 2020, **19**, 1047–1056.
102 M. Ravi, V. L. Sushkevich and J. A. van Bokhoven, *J. Phys. Chem. C*, 2019, **123**, 15139–15144.
103 M. Ravi, V. L. Sushkevich and J. A. van Bokhoven, *Chem. Sci.*, 2021, **12**, 4094–4103.
104 A. V. Yakimov, M. Ravi, R. Verel, V. L. Sushkevich, J. A. van Bokhoven and C. Copéret, *J. Am. Chem. Soc.*, 2022, **144**, 10377–10385.
105 X. Yi, K. Liu, W. Chen, J. Li, S. Xu, C. Li, Y. Xiao, H. Liu, X. Guo, S.-B. Liu and A. Zheng, *J. Am. Chem. Soc.*, 2018, **140**, 10764–10774.
106 K. Chen, Z. Gan, S. Horstmeier and J. L. White, *J. Am. Chem. Soc.*, 2021, **143**, 6669–6680.
107 M. Hu, C. Wang, Y. Chu, Q. Wang, S. Li, J. Xu and F. Deng, *Angew. Chem., Int. Ed.*, 2022, **61**, e202207400.
108 Z. Wang, D. Xiao, K. Chen, C. Lou, L. Liang, S. Xu and G. Hou, *ACS Catal.*, 2023, **13**, 4960–4970.
109 S. Shetty, B. S. Kulkarni, D. G. Kanhere, A. Goursot and S. Pal, *J. Phys. Chem. B*, 2008, **112**, 2573–2579.
110 R. Gounder and M. E. Davis, *AIChE J.*, 2013, **59**, 3349–3358.
111 N. A. Grosso-Giordano, A. S. Hoffman, A. Boubnov, D. W. Small, S. R. Bare, S. I. Zones and A. Katz, *J. Am. Chem. Soc.*, 2019, **141**, 7090–7106.
112 V. Choudhary, A. B. Pinar, S. I. Sandler, D. G. Vlachos and R. F. Lobo, *ACS Catal.*, 2011, **1**, 1724–1728.
113 R. Gounder and M. E. Davis, *J. Catal.*, 2013, **308**, 176–188.
114 J. W. Harris, M. J. Cordon, J. R. Di Iorio, J. C. Vega-Vila, F. H. Ribeiro and R. Gounder, *J. Catal.*, 2016, **335**, 141–154.
115 L. Botti, S. A. Kondrat, R. Navar, D. Padovan, J. S. Martinez-Espin, S. Meier and C. Hammond, *Angew. Chem., Int. Ed.*, 2020, **59**, 20017–20023.
116 J. S. Bates and R. Gounder, *J. Catal.*, 2018, **365**, 213–226.
117 J. S. Bates, B. C. Bukowski, J. W. Harris, J. Greeley and R. Gounder, *ACS Catal.*, 2019, **9**, 6146–6168.
118 A. Corma, L. T. Nemeth, M. Renz and S. Valencia, *Nature*, 2001, **412**, 423–425.
119 J. D. Lewis, S. V. de Vyver and Y. Román-Leshkov, *Angew. Chem., Int. Ed.*, 2015, **54**, 9835–9838.
120 J. J. Pacheco and M. E. Davis, *Proc. Nat. Acad. Sci. U. S. A.*, 2014, **111**, 8363–8367.
121 T. Blasco, M. A. Camblor, A. Corma, P. Esteve, J. M. Guil, A. Martínez, J. A. Perdigón-Melón and S. Valencia, *J. Phys. Chem. B*, 1998, **102**, 75–88.
122 B. C. Bukowski, J. S. Bates, R. Gounder and J. Greeley, *Angew. Chem., Int. Ed.*, 2019, **58**, 16422–16426.
123 E. Gallo, F. Bonino, J. C. Swarbrick, T. Petrenko, A. Piovano, S. Bordiga, D. Gianolio, E. Groppo, F. Neese, C. Lamberti and P. Glatzel, *ChemPhysChem*, 2013, **14**, 79–83.
124 P. Wolf, M. Valla, A. J. Rossini, A. Comas-Vives, F. Núñez-Zarur, B. Malaman, A. Lesage, L. Emsley, C. Copéret and I. Hermans, *Angew. Chem., Int. Ed.*, 2014, **53**, 10179–10183.
125 M. J. Cordon, J. W. Harris, J. C. Vega-Vila, J. S. Bates, S. Kaur, M. Gupta, M. E. Witzke, E. C. Wegener, J. T. Miller, D. W. Flaherty, D. D. Hibbitts and R. Gounder, *J. Am. Chem. Soc.*, 2018, **140**, 14244–14266.
126 D. T. Bregante, M. C. Chan, J. Z. Tan, E. Z. Ayla, C. P. Nicholas, D. Shukla and D. W. Flaherty, *Nat. Catal.*, 2021, **4**, 797–808.
127 T. D. Courtney, C.-C. Chang, R. J. Gorte, R. F. Lobo, W. Fan and V. Nikolakis, *Micro. Meso. Mater.*, 2015, **210**, 69–76.
128 D. T. Bregante, D. S. Potts, O. Kwon, E. Z. Ayla, J. Z. Tan and D. W. Flaherty, *Chem. Mater.*, 2020, **32**, 7425–7437.
129 J. C. Vega-Vila and R. Gounder, *ACS Catal.*, 2020, **10**, 12197–12211.
130 D. S. Potts, V. S. Jeyaraj, O. Kwon, R. Ghosh, A. V. Mironenko and D. W. Flaherty, *ACS Catal.*, 2022, **12**, 13372–13393.
131 A. G. Panov and J. J. Fripiat, *Catal. Lett.*, 1999, **57**, 25–32.
132 V. Bolis, J. C. Vedrine, J. P. Van de Berg, J. P. Wolthuizen and E. G. Derouane, *J. Chem. Soc., Faraday Trans., 1*, 1980, **76**, 1606–1616.
133 H. Wang, Y. Hou, W. Sun, Q. Hu, H. Xiong, T. Wang, B. Yan and W. Qian, *ACS Catal.*, 2020, **10**, 5288–5298.
134 K. De Wispelaere, C. S. Wondergem, B. Ensing, K. Hemelsoet, E. J. Meijer, B. M. Weckhuysen, V. V. Speybroeck and J. Ruiz-Martinez, *ACS Catal.*, 2016, **6**, 1991–2002.

 

135 J. Valecillos, G. Elordi, A. T. Aguayo and P. Castaño, *Catal. Sci. Technol.*, 2021, **11**, 1269–1281.
136 X. Zhao, J. Li, P. Tian, L. Wang, X. Li, S. Lin, X. Guo and Z. Liu, *ACS Catal.*, 2019, **9**, 3017–3025.
137 C. Wang, L. Yang, M. Gao, X. Shao, W. Dai, G. Wu, N. Guan, Z. Xu, M. Ye and L. Li, *J. Am. Chem. Soc.*, 2022, **144**, 21408–21416.
138 J. Gil-Coba, S. C. Marie-Rose and J.-M. Lavoie, *Catal. Lett.*, 2016, **146**, 2534–2542.
139 R. Brosius, P. J. Kooyman and J. C. Q. Fletcher, *ACS Catal.*, 2016, **6**, 7710–7715.
140 A. Corma, O. Marie and F. J. Ortega, *J. Catal.*, 2004, **222**, 338–347.
141 P. Bollini, T. T. Chen, M. Neurock and A. Bhan, *Catal. Sci. Technol.*, 2019, **9**, 4374–4383.
142 S. A. F. Nastase, P. Cnudde, L. Vanduyfhuys, K. De Wispelaere, V. Van Speybroeck, C. R. A. Catlow and A. J. Logsdail, *ACS Catal.*, 2020, **10**, 8904–8915.
143 D. T. Bregante and D. W. Flaherty, *ACS Catal.*, 2019, **9**, 10951–10962.
144 S. Eckstein, P. H. Hintermeier, M. V. Olarte, Y. Liu, E. Baráth and J. A. Lercher, *J. Catal.*, 2017, **352**, 329–336.
145 N. S. Gould and B. Xu, *ACS Catal.*, 2018, **8**, 8699–8708.
146 N. S. Gould, S. Li, H. J. Cho, H. Landfield, S. Caratzoulas, D. Vlachos, P. Bai and B. Xu, *Nat. Commun.*, 2020, **11**, 1060.
147 K. Chen, J. Damron, C. Pearson, D. Resasco, L. Zhang and J. L. White, *ACS Catal.*, 2014, **4**, 3039–3044.
148 K. Chen, A. Gumidyala, M. Abdolrhamani, C. Villines, S. Crossley and J. L. White, *J. Catal.*, 2017, **351**, 130–135.
149 M. Bocus, L. Vanduyfhuys, F. De Proft, B. M. Weckhuysen and V. Van Speybroeck, *JACS Au*, 2022, **2**, 502–514.
150 Y. Zhi, H. Shi, L. Mu, Y. Liu, D. Mei, D. M. Camaioni and J. A. Lercher, *J. Am. Chem. Soc.*, 2015, **137**, 15781–15794.
151 M. Gešvandtnerová, T. Bučko, P. Raybaud and C. Chizallet, *J. Catal.*, 2022, **413**, 786–802.
152 H. K. Chau, H. D. Mai, A. Gumidyala, T. N. Pham, D.-P. Bui, A. D. D'Amico, I. Alalq, D. T. Glatzhofer, J. L. White and S. P. Crossley, *ACS Catal.*, 2023, **13**, 9158–9170.
153 C. Wang, Y. Chu, D. Xiong, H. Wang, M. Hu, Q. Wang, J. Xu and F. Deng, *Angew. Chem., Int. Ed.*, 2024, **63**, e202313974.
154 M. Bocus and V. Van Speybroeck, *ACS Catal.*, 2022, **12**, 14227–14242.
155 W. N. P. van der Graaff, C. H. L. Tempelman, G. Li, B. Mezari, N. Kosinov, E. A. Pidko and E. J. M. Hensen, *ChemSusChem*, 2016, **9**, 3145–3149.
156 H. K. Chau, Q. P. Nguyen, A. C. Jerdy, D.-P. Bui, L. L. Lobban, B. Wang and S. P. Crossley, *ACS Catal.*, 2023, **13**, 1503–1512.
157 Y. Liu, A. Vjunov, H. Shi, S. Eckstein, D. M. Camaioni, D. Mei, E. Baráth and J. A. Lercher, *Nat. Commun.*, 2017, **8**, 14113.
158 H. Shi, S. Eckstein, A. Vjunov, D. M. Camaioni and J. A. Lercher, *Nat. Commun.*, 2017, **8**, 15442.
159 M. Shetty, H. Wang, F. Chen, N. Jaegers, Y. Liu, D. M. Camaioni, O. Y. Gutiérrez and J. A. Lercher, *Angew. Chem., Int. Ed.*, 2021, **60**, 2304–2311.
160 L. Milaković, P. H. Hintermeier, Y. Liu, E. Baráth and J. A. Lercher, *Angew. Chem., Int. Ed.*, 2021, **60**, 24806–24810.
161 Q. Liu, N. Pfriem, G. Cheng, E. Baráth, Y. Liu and J. A. Lercher, *Angew. Chem., Int. Ed.*, 2023, **62**, e202208693.
162 D. T. Bregante, A. M. Johnson, A. Y. Patel, E. Z. Ayla, M. J. Cordon, B. C. Bukowski, J. Greeley, R. Gounder and D. W. Flaherty, *J. Am. Chem. Soc.*, 2019, **141**, 7302–7319.
163 Y. Chu, X. Yi, C. Li, X. Sun and A. Zheng, *Chem. Sci.*, 2018, **9**, 6470–6479.
164 K. Chen, M. Abdolrahmani, S. Horstmeier, T. N. Pham, V. T. Nguyen, M. Zeets, B. Wang, S. Crossley and J. L. White, *ACS Catal.*, 2019, **9**, 6124–6136.
165 Y. Zhang, R. Zhao, M. Sanchez-Sanchez, G. L. Haller, J. Hu, R. Bermejo-Deval, Y. Liu and J. A. Lercher, *J. Catal.*, 2019, **370**, 424–433.
166 T. N. Pham, V. Nguyen, B. Wang, J. L. White and S. Crossley, *ACS Catal.*, 2021, **11**, 6982–6994.
167 S. Li, A. Zheng, Y. Su, H. Zhang, L. Chen, J. Yang, C. Ye and F. Deng, *J. Am. Chem. Soc.*, 2007, **129**, 11161–11171.
168 C. Liu, G. Li, E. J. M. Hensen and E. A. Pidko, *ACS Catal.*, 2015, **5**, 7024–7033.
169 C. Liu, G. Li, E. J. M. Hensen and E. A. Pidko, *J. Catal.*, 2016, **344**, 570–577.
170 M. Niwa, K. Suzuki, N. Morishita, G. Sastre, K. Okumura and N. Katada, *Catal. Sci. Technol.*, 2013, **3**, 1919–1927.
171 C. Chizallet, C. Bouchy, K. Larmier and G. Pirngruber, *Chem. Rev.*, 2023, **123**, 6107–6196.
172 A. Vjunov, M. A. Derewinski, J. L. Fulton, D. M. Camaioni and J. A. Lercher, *J. Am. Chem. Soc.*, 2015, **137**, 10374–10382.
173 J. T. C. Wennmacher, S. Mahmoudi, P. Rzepka, S. S. Lee, T. Gruene, V. Paunović and J. A. van Bokhoven, *Angew. Chem., Int. Ed.*, 2022, **61**, e202205413.
174 Y. Wei, C. Yuan, J. Li, S. Xu, Y. Zhou, J. Chen, Q. Wang, L. Xu, Y. Qi, Q. Zhang and Z. Liu, *ChemSusChem*, 2012, **5**, 906–912.
175 Y. Nakasaka, J.-i Nishimura, T. Tago and T. Masuda, *Chem. Eng. J.*, 2015, **278**, 159–165.
176 N. Kosinov, E. A. Uslamin, F. J. A. G. Coumans, A. S. G. Wijpkema, R. Y. Rohling and E. J. M. Hensen, *ACS Catal.*, 2018, **8**, 8459–8467.
177 D. Kiani, S. Sourav, Y. Tang, J. Baltrusaitis and I. E. Wachs, *Chem. Soc. Rev.*, 2021, **50**, 1251–1268.
178 M. Luo, Y. Fu, B. Hu, D. Wang, B. Wang and G. Mao, *Appl. Catal., A*, 2019, **570**, 209–217.
179 X. Wu and R. G. Anthony, *Appl. Catal., A*, 2001, **218**, 241–250.
180 H. An, F. Zhang, Z. Guan, X. Liu, F. Fan and C. Li, *ACS Catal.*, 2018, **8**, 9207–9215.
181 L. Yang, C. Wang, L. Zhang, W. Dai, Y. Chu, J. Xu, G. Wu, M. Gao, W. Liu, Z. Xu, P. Wang, N. Guan, M. Dyballa, M. Ye, F. Deng, W. Fan and L. Li, *Nat. Commun.*, 2021, **12**, 4661.
182 E. Catizzone, M. Migliori, A. Purita and G. Giordano, *J. Energy Chem.*, 2019, **30**, 162–169.
183 M. Çağlayan, A. L. Paioni, B. Dereli, G. Shterk, I. Hita, E. Abou-Hamad, A. Pustovarenko, A.-H. Emwas, A. Dikhtiarenko,

P. Castaño, L. Cavallo, M. Baldus, A. D. Chowdhury and J. Gascon, *ACS Catal.*, 2021, **11**, 11671–11684.
184 A. Vjunov, J. L. Fulton, D. M. Camaioni, J. Z. Hu, S. D. Burton, I. Arslan and J. A. Lercher, *Chem. Mater.*, 2015, **27**, 3533–3545.
185 L. Zhang, K. Chen, B. Chen, J. L. White and D. E. Resasco, *J. Am. Chem. Soc.*, 2015, **137**, 11810–11819.
186 S. Prodinger, H. Shi, S. Eckstein, J. Z. Hu, M. V. Olarte, D. M. Camaioni, M. A. Derewinski and J. A. Lercher, *Chem. Mater.*, 2017, **29**, 7255–7262.
187 S. Prodinger, H. Shi, H. Wang, M. A. Derewinski and J. A. Lercher, *Appl. Catal., B*, 2018, **237**, 996–1002.
188 M. Boronat, P. Concepción, A. Corma, M. Renz and S. Valencia, *J. Catal.*, 2005, **234**, 111–118.
189 V. L. Sushkevich, P. A. Kots, Y. G. Kolyagin, A. V. Yakimov, A. V. Marikutsa and I. I. Ivanova, *J. Phys. Chem. C*, 2019, **123**, 5540–5548.
190 G. Qi, Q. Wang, J. Xu, Q. Wu, C. Wang, X. Zhao, X. Meng, F. Xiao and F. Deng, *Commun. Chem.*, 2018, **1**, 22.
191 G. Li, E. A. Pidko and E. J. M. Hensen, *Catal. Sci. Technol.*, 2014, **4**, 2241–2250.
192 D. Padovan, L. Botti and C. Hammond, *ACS Catal.*, 2018, **8**, 7131–7140.
193 M. J. Cordon, J. N. Hall, J. W. Harris, J. S. Bates, S.-J. Hwang and R. Gounder, *Catal. Sci. Technol.*, 2019, **9**, 1654–1668.
194 L. Treps, A. Gomez, T. de Bruin and C. Chizallet, *ACS Catal.*, 2020, **10**, 3297–3312.
195 J. Rey, P. Raybaud and C. Chizallet, *ChemCatChem*, 2017, **9**, 2176–2185.
196 L. Treps, C. Demaret, D. Wisser, B. Harbuzaru, A. Méthivier, E. Guillon, D. V. Benedis, A. Gomez, T. de Bruin, M. Rivallan, L. Catita, A. Lesage and C. Chizallet, *J. Phys. Chem. C*, 2021, **125**, 2163–2181.
197 T. Jarrin, T. de Bruin and C. Chizallet, *ChemCatChem*, 2023, **15**, e202201302.
198 C. Chizallet, *ACS Catal.*, 2020, **10**, 5579–5601.
199 G. Agostini, C. Lamberti, L. Palin, M. Milanesio, N. Danilina, B. Xu, M. Janousch and J. A. van Bokhoven, *J. Am. Chem. Soc.*, 2010, **132**, 667–678.
200 J. Zhou, M. Gao, J. Zhang, W. Liu, T. Zhang, H. Li, Z. Xu, M. Ye and Z. Liu, *Nat. Commun.*, 2021, **12**, 17.
201 T. Sun, S. Xu, D. Xiao, Z. Liu, G. Li, A. Zheng, W. Liu, Z. Xu, Y. Cao, Q. Guo, N. Wang, Y. Wei and Z. Liu, *Angew. Chem., Int. Ed.*, 2020, **59**, 20672–20681.
202 A. Zornes, N. B. Abdul Rahman, O. R. Das, L. A. Gomez, S. Crossley, D. E. Resasco and J. L. White, *J. Am. Chem. Soc.*, 2024, **146**, 1132–1143.
203 J. A. van Bokhoven, D. C. Koningsberger, P. Kunkeler, H. van Bekkum and A. P. M. Kentgens, *J. Am. Chem. Soc.*, 2000, **122**, 12842–12847.
204 M. Signorile, F. Bonino, A. Damin and S. Bordiga, *J. Phys. Chem. C*, 2016, **120**, 18088–18092.
205 B. Fan, D. Zhu, L. Wang, S. Xu, Y. Wei and Z. Liu, *Inorg. Chem. Front.*, 2022, **9**, 3609–3618.
206 X. Bai, J. Zhang, C. Liu, S. Xu, Y. Wei and Z. Liu, *Micro. Meso. Mater.*, 2023, **354**, 112555.
207 T. Blasco, A. Corma and J. Martínez-Triguero, *J. Catal.*, 2006, **237**, 267–277.
208 S. M. C. Menezes, V. L. Camorim, Y. L. Lam, R. A. S. San Gil, A. Bailly and J. P. Amoureux, *Appl. Catal., A*, 2001, **207**, 367–377.
209 A. G. Gayubo, A. T. Aguayo, A. Atutxa, R. Prieto and J. Bilbao, *Ind. Eng. Chem. Res.*, 2004, **43**, 5042–5048.
210 S. M. T. Almutairi, B. Mezari, E. A. Pidko, P. C. M. M. Magusin and E. J. M. Hensen, *J. Catal.*, 2013, **307**, 194–203.
211 L. R. Aramburo, E. de Smit, B. Arstad, M. M. van Schooneveld, L. Sommer, A. Juhin, T. Yokosawa, H. W. Zandbergen, U. Olsbye, F. M. F. de Groot and B. M. Weckhuysen, *Angew. Chem., Int. Ed.*, 2012, **51**, 3616–3619.
212 B. Xu, F. Rotunno, S. Bordiga, R. Prins and J. A. van Bokhoven, *J. Catal.*, 2006, **241**, 66–73.
213 J. A. van Bokhoven, A. M. J. van der Eerden and D. C. Koningsberger, *Stud. Surf. Sci. Catal.*, 2002, **142**, 1885–1890.
214 J. A. van Bokhoven, A. M. J. van der Eerden and D. C. Koningsberger, *J. Am. Chem. Soc.*, 2003, **125**, 7435–7442.
215 M. Jin, M. Ravi, C. Lei, C. J. Heard, F. Brivio, Z. Tošner, L. Grajciar, J. A. van Bokhoven and P. Nachtigall, *Angew. Chem., Int. Ed.*, 2023, **62**, e202306183.
216 A. Omegna, J. A. van Bokhoven and R. Prins, *J. Phys. Chem. B*, 2003, **107**, 8854–8860.
217 Y. Ma, J. Ding, L. Yang, X. Wu, Y. Gao, R. Ran and D. Weng, *J. Phys. Chem. C*, 2023, **127**, 16598–16606.
218 M.-C. Silaghi, C. Chizallet, J. Sauer and P. Raybaud, *J. Catal.*, 2016, **339**, 242–255.
219 S. Malola, S. Svelle, F. L. Bleken and O. Swang, *Angew. Chem., Int. Ed.*, 2012, **51**, 652–655.
220 M.-C. Silaghi, C. Chizallet, E. Petracovschi, T. Kerber, J. Sauer and P. Raybaud, *ACS Catal.*, 2015, **5**, 11–15.
221 M. Nielsen, A. Hafreager, R. Y. Brogaard, K. De Wispelaere, H. Falsig, P. Beato, V. V. Speybroeck and S. Svelle, *Catal. Sci. Technol.*, 2019, **9**, 3721–3725.
222 K. Stanciakova, B. Ensing, F. Göltl, R. E. Bulo and B. M. Weckhuysen, *ACS Catal.*, 2019, **9**, 5119–5135.
223 C. J. Heard, L. Grajciar, C. M. Rice, S. M. Pugh, P. Nachtigall, S. E. Ashbrook and R. E. Morris, *Nat. Commun.*, 2019, **10**, 4690.
224 S. M. Pugh, P. A. Wright, D. J. Law, N. Thompson and S. E. Ashbrook, *J. Am. Chem. Soc.*, 2020, **142**, 900–906.
225 F. Lin, M. Xu, K. K. Ramasamy, Z. Li, J. L. Klinger, J. A. Schaidle and H. Wang, *ACS Catal.*, 2022, **12**, 13555–13599.
226 R. M. Ravenelle, F. Schüβler, A. D'Amico, N. Danilina, J. A. van Bokhoven, J. A. Lercher, C. W. Jones and C. Sievers, *J. Phys. Chem. C*, 2010, **114**, 19582–19595.
227 A. R. Maag, G. A. Tompsett, J. Tam, C. A. Ang, G. Azimi, A. D. Carl, X. Huang, L. J. Smith, R. L. Grimm, J. Q. Bond and M. T. Timko, *Phys. Chem. Chem. Phys.*, 2019, **21**, 17880–17892.
228 T. Ennaert, J. Geboers, E. Gobechiya, C. M. Courtin, M. Kurttepeli, K. Houthoofd, C. E. A. Kirschhock,

 

P. C. M. M. Magusin, S. Bals, P. A. Jacobs and B. F. Sels, *ACS Catal.*, 2015, **5**, 754–768.
229 C. E. Hernandez-Tamargo, A. Roldan and N. H. de Leeuw, *J. Solid State Chem.*, 2016, **237**, 192–203.
230 F. Dubray, E. Dib, I. Medeiros-Costa, C. Aquino, D. Minoux, S. van Daele, N. Nesterenko, J.-P. Gilson and S. Mintova, *Inorg. Chem. Front.*, 2022, **9**, 1125–1133.
231 G. M. Lari, P. Y. Dapsens, D. Scholz, S. Mitchell, C. Mondelli and J. Pérez-Ramírez, *Green Chem.*, 2016, **18**, 1249–1260.
232 C. J. Heard, L. Grajciar, F. Uhlík, M. Shamzhy, M. Opanasenko, J. Čejka and P. Nachtigall, *Adv. Mater.*, 2020, **32**, 2003264.
233 J. N. Louwen, S. Simko, K. Stanciakova, R. E. Bulo, B. M. Weckhuysen and E. T. C. Vogt, *J. Phys. Chem. C*, 2020, **124**, 4626–4636.
234 J. Sun, H. Fang, P. I. Ravikovitch and D. S. Sholl, *J. Phys. Chem. C*, 2020, **124**, 668–676.
235 R. C. Shiery, S. J. McElhany and D. C. Cantu, *J. Phys. Chem. C*, 2021, **125**, 13649–13657.
236 G. Caeiro, P. Magnoux, J. M. Lopes, F. R. Ribeiro, S. M. C. Menezes, A. F. Costa and H. S. Cerqueira, *Appl. Catal., B*, 2006, **314**, 160–171.
237 A. Corma, J. Mengual and P. J. Miguel, *Appl. Catal., A*, 2012, **421–422**, 121–134.
238 Y. Kakiuchi, T. Tanigawa, N. Tsunoji, Y. Takamitsu, M. Sadakane and T. Sano, *Appl. Catal., A*, 2019, **575**, 204–213.
239 R. Simancas, A. Chokkalingam, S. P. Elangovan, Z. Liu, T. Sano, K. Iyoki, T. Wakihara and T. Okubo, *Chem. Sci.*, 2021, **12**, 7677.
240 H. E. Van der Bij and B. M. Weckhuysen, *Phys. Chem. Chem. Phys.*, 2014, **16**, 9892–9903.
241 H. Vinek, G. Rumplmayr and J. A. Lercher, *J. Catal.*, 1989, **115**, 291–300.
242 G. Lischke, R. Eckelt, H.-G. Jerschkewitz, B. Parlitz, E. Schreier, W. Storek, B. Zibrowius and G. Öhlmann, *J. Catal.*, 1991, **132**, 229–243.
243 H. E. Van der Bij and B. M. Weckhuysen, *Chem. Soc. Rev.*, 2015, **44**, 7406–7428.
244 J. N. Louwen, L. van Eijck, C. Vogt and E. T. C. Vogt, *Chem. Mater.*, 2020, **32**, 9390–9403.
245 U. Khalil, O. Muraza, H. Kondoh, G. Watanabe, Y. Nakasaka, A. Al-Amer and T. Masuda, *Fuel*, 2006, **168**, 61–67.
246 Y. Wang, P. Guerra, A. Zaker, A. R. Maag, G. A. Tompsett, L. J. Smith, X. Huang, J. Q. Bond and M. T. Timko, *ACS Catal.*, 2020, **10**, 6623–6634.
247 P. A. Zapata, J. Faria, M. P. Ruiz, R. E. Jentoft and D. E. Resasco, *J. Am. Chem. Soc.*, 2012, **134**, 8570–8578.
248 P. A. Zapata, Y. Huang, M. A. Gonzalez-Borja and D. E. Resasco, *J. Catal.*, 2013, **308**, 82–97.
249 S. Prodinger, M. A. Derewinski, A. Vjunov, S. D. Burton, I. Arslan and J. A. Lercher, *J. Am. Chem. Soc.*, 2016, **138**, 4408–4415.
250 M. A. Camblor, A. Corma and S. Valencia, *J. Mater. Chem.*, 1998, **8**, 2137–2145.
251 J. Saavedra, H. A. Doan, C. J. Pursell, L. C. Grabow and B. D. Chandler, *Science*, 2014, **345**, 1599–1602.
252 L. Lin, W. Zhou, R. Gao, S. Yao, X. Zhang, W. Xu, S. Zheng, Z. Jiang, Q. Yu, Y.-W. Li, C. Shi, X.-D. Wen and D. Ma, *Nature*, 2017, **544**, 80–83.
253 Z. Liu, E. Huang, I. Orozco, W. Liao, R. M. Palomino, N. Rui, T. Duchoň, S. Nemšák, D. C. Grinter, M. Mahapatra, P. Liu, J. A. Rodriguez and S. D. Senanayake, *Science*, 2020, **368**, 513–517.
254 K. Xu, Y. Chen, H. Yang, Y. Gan, L. Wu, L. Tan, Y. Dai and Y. Tang, *Appl. Catal., B*, 2024, **341**, 123244.
255 H. Shi, J. A. Lercher and X.-Y. Yu, *Catal. Sci. Technol.*, 2015, **5**, 3035–3060.
256 N. S. Gould and B. Xu, *Chem. Sci.*, 2018, **9**, 281–287.
257 G. Noh, Z. Shi, S. I. Zones and E. Iglesia, *J. Catal.*, 2018, **368**, 389–410.
258 V. Shostak, E. Redekop and U. Olsbye, *Catal. Today*, 2023, **417**, 113785.
259 P. Cnudde, R. Demuynck, S. Vandenbrande, M. Waroquier, G. Sastre and V. Van Speybroeck, *J. Am. Chem. Soc.*, 2020, **142**, 6007–6017.
260 V. Van Speybroeck, M. Bocus, P. Cnudde and L. Vanduyfhuys, *ACS Catal.*, 2023, **13**, 11455–11493.